NTNU – Trondheim
Norwegian University of
Science and Technology

High pressure equation of state for condensed phase thermodynamics

Stig-Erik Nogva

Chemical Engineering and Biotechnology
Submission date: June 2012
Supervisor: Tore Haug-Warberg, IKP

Norwegian University of Science and Technology
Department of Chemical Engineering

I declare that this is an independent work according to the exam regulations of the Norwegian University of Science and Technology.

Trondheim, June 15, 2012

Stig-Erik Nogva

Abstract

In this study a search for an equation of state (EOS) that accurately predicts solids behaviour at both high pressure and temperature has been performed. Firstly, several two-parameter isothermal EOSs for solids under high pressure were investigated. The EOSs evaluated were the Murnaghan, Birch–Murnaghan, Vinet and pseudo-spinodal. The input parameters needed were found through parameter fitting of experimental data. The parameter fitting was done through a second order Murnaghan equation on implicit form. This equation was found through an integration of a Taylor expansion in pressure of the bulk modulus. The parameters obtained were the isothermal bulk modulus, and its first and second pressure derivative for each solid in question.

The solids investigated were the low pressure forms of MgO (periclase), CaO (lime), Al_2O_3 (corundum), SiO_2 (α-quartz), NaCl (halite) and $MgCO_3$ (magnesite). The names given in parenthesis are the names of the minerals found naturally on Earth. The experimental data found in the literature is from measurements on synthetically produced solids, but the data is often used to represent the natural mineral as well.

In order to test the two-parameter EOSs against each other, the standard deviations for the parameters were needed. The standard deviation was found through bootstrapping and maximum likelihood, i.e. two different statistical methods. These two methods gave comparable results for the standard deviation of the parameters ($\pm 5 - 65\%$) except for MgO, which was found to reject the null hypothesis of normal distribution based on a χ^2-test. Thus, the optimal parameters were reported using the bootstrap method, which is distribution independent. The optimal parameters obtained, including their uncertainties, were then used to test which of the two-parameter EOSs give the best fit to experimental data.

Based on the analysis completed in this study, all the EOSs tested, except the first order Murnaghan were close to the standard deviation for all the different solids investigated at

high pressure. Thus, a general conclusion on which EOS that gave the best fit for all the solids examined could not be drawn. Nevertheless, the pseudo-spinodal EOS has some promising features when it comes to high temperature and high pressure predictions, and was therefore used to model the complete pressure-volume-temperature surface.

Predictions of the heat capacities, thermal expansion and the isothermal bulk modulus at high pressure and temperature for NaCl and MgO were done based on the pseudo-spinodal EOS. The thermal expansion and the complete pressure-volume-temperature surface predicted were also compared with available experimental data. The predictions give good fit to the data. However, from this analysis it may seem that the pseudo-spinodal EOS gives better fit for alkali halides than for oxides due to the difference in thermal dependency of the Grüneisen parameter for these two substance groups. For alkali halides, e.g. NaCl, the Grüneisen parameter generally decreases with temperature. For oxides on the other hand, e.g. MgO, the Grüneisen parameter increases with temperature. This opposite temperature effect on the Grüneisen parameter for oxides and alkali halides has implications on the model predictions within the framework of the pseudo-spinodal EOS.

The major finding in this report was that an inconsistency in the pseudo-spinodal EOS was found at high pressure. This EOS predicts negative heat capacity at very high pressures and low temperatures. It is recommended in further work to search for a consistent way of including internal energy. This will provide an EOS of great value in the prediction of high pressure and high temperature effects on solids.

Sammendrag

I denne studien ble et søk etter en tilstandsligning som presist predikerer faste stoffers oppførsel ved både høyt trykk og høy temperatur utført. Først ble flere to-parameter isoterme tilstandsligninger for faste stoffer under høyt trykk undersøkt. Tilstandsligningene som ble undersøkt var Murnaghan, Birch–Murnaghan, Vinet og pseudo-spinodal. Parameterne som trengtes for tilstandsligningene ble funnet gjennom parametertilpasning av eksperimentelle data. Parametertilpasningen ble gjort ved hjelp av en andreordens Murnaghan ligning på implisitt form. Denne ligningen ble funnet ved integrasjon av en Taylor rekkeutvikling i trykk av bulk modulus. Parameterne som ble funnet var den isoterme bulk modulus, og dens første og andre deriverte med hensyn på trykk for hvert av de faste stoffene som ble undersøkt.

De faste stoffene som ble undersøkt var lavtrykksformene av MgO (periclase), CaO (lime), Al_2O_3 (corundum), SiO_2 (α-quartz), NaCl (halite) and $MgCO_3$ (magnesite). Navnene i parentes er navnene til mineralene slik de blir funnet naturlig på jorden. De eksperimentelle dataene som er funnet i litteraturen er fra målinger på syntetisk fremstilte faste stoffer, men disse dataene blir også ofte brukt til å representere de naturlige mineralene.

For å ha muligheten til å teste de to-parameter tilstandsligningene mot hverandre trengtes standardavviket for parametrene. Dette ble funnet ved hjelp av bootstrap og maximum likelihood, det vil si to forskjellige statistiske metoder. Disse to metodene gav sammenlignbare resultater for standardavviket for parametrene ($\pm 5 - 65\%$) utenom for MgO som avviste nullhypotesen for normalfordeling basert på en χ^2-test. De optimale parametrene ble derfor rapportert ved bruk av bootstrap metoden som er fordelingsuavhengig. Optimal parametrene som ble funnet, inkludert deres usikkerheter, ble deretter brukt til å finne hvilken av de to-parameter tilstandsligningene som gav den beste tilpasningen til eksperimentelle data.

Basert på analysen utført i denne studien var alle tilstandsligningene som ble testet, utenom førsteordens Murnaghan, nærme standardavviket for alle de undersøkte faste stoffene ved høye trykk. En generell konklusjon for hvilken tilstandsligning som gav best tilpasning kunne derfor ikke bli trukket. Den pseudo-spinodale tilstandsligningen har likevel noen lovende attributter når det kommer til prediksjoner ved høy temperatur og trykk. Denne ligningen ble derfor brukt til å modellere hele trykk-volum-temperatur flaten.

Prediksjoner av varmekapasitet, termisk ekspansjon og den isoterme bulk modulusen ved høyt trykk og temperatur for NaCl og MgO ble gjort basert på den pseudo-spinodale tilstandsligningen. Prediksjonene av termisk ekspansjon og den totale trykk-volum-temperatur flaten ble også sammenlignet med eksperimentelle data. Prediksjonene gav god tilpasning til dataene. Det kan fra denne analysen imidlertid se ut som den pseudo-spinodale tilstandsligningen gir bedre tilpasning for alkali halider enn for oksider på grunn av ulik termisk avhengighet for Grüneisen parameteren for disse to stoffgruppene. For alkali halider, for eksempel NaCl, Grüneisen parameteren generelt synker når temperaturen synker. For oksider derimot, for eksempel MgO, Grüneisen parameteren øker når temperaturen synker. Denne motsatte temperatureffekten for Grüneisen parameteren for disse to stoffgruppene gir ulik tilpasningspresisjon innenfor rammeverket til den pseudo-spinodale tilstandsligningen.

Den viktigste oppdagelsen i denne rapporten var en inkonsistens i den pseudo-spinodale tilstandsligningen. Denne tilstandsligningen predikerte negativ varmekapasitet ved høye trykk og lave temperaturer. Det er anbefalt i videre arbeid å lete etter en konsistent måte for å inkludere indre energi. Dette vil gi en tilstandsligning av stor verdi for prediksjoner av høye trykk og høy temperatur effekter på faste stoffer.

Acknowledgments

After five years of studies at NTNU in Trondheim my final year has now come to an end. I have learned a lot through these years as a student, and this thesis is the conclusive work of my Master of Science degree at the Department of Chemical Engineering. This work would not have been possible without the help and encouragement of others.

I am indebted to Associate professor Tore Haug-Warberg, my supervisor, for his patience and eager to teach me some of his vast knowledge in thermodynamics. Without his assistance and feedback this thesis would not have been possible. I am also very grateful for the interest he has shown in my work.

Further, I would like to thank my family for all the support they have given me through these years. They have been a sturdy rock in my life and someone I always have been able to rely on.

Finally, I would like to thank my friends and fellow students.

Contents

Abstract v

Sammendrag vii

Acknowledgments ix

List of Symbols xiii

1 Introduction 1

2 Theory 3

2.1 Physical properties and thermoelastic parameters 3

2.2 Isothermal equations of state 6

2.3 Derivations of the isothermal EOSs 8

2.3.1 Murnaghan 8

2.3.2 Vinet 8

2.3.3 Birch–Murnaghan 9

2.3.4 Pseudo-spinodal 11

2.4 Incorporation of thermal effects 12

2.5 Derivation of chemical potential 14

2.6 Statistics 17

3 Literature study 19

4 Results 21

4.1 Parameter fitting 21

4.2 Deviation plots 24

4.3 Predictions at high temperature and pressure 29

5 Discussion **35**
5.1 Parameter fit compared with literature values 35
5.2 Isothermal EOSs and uncertainty vectors 36
5.3 The complete EOS and comparison with experimental data 38
5.4 Chi-square goodness of fit test 44

6 Conclusion **47**

A Pressure-volume data for the isothermal curve fitting **55**

B Matlab code **69**
B.1 Data management 69
B.2 Implementation of the second order Murnaghan on implicit form 71
B.3 Parameter fitting 71
B.4 The bootstrap method 73
B.5 Deviation plots 76
B.6 Isobaric heat capacity as a function of temperature 80
B.7 Isobaric heat capacity as a function of pressure 83
B.8 Bulk modulus as a function of temperature 86
B.9 Bulk modulus as a function of pressure 88
B.10 Thermal expansion as a function of temperature 90
B.11 Thermal expansion as a function of pressure 91
B.12 Comparison of the thermal expansion with experimental data 93
B.13 Comparison of the p-V-T surface with experimental data for MgO 95
B.14 Calculation of the Chi-square value for MgO 97

List of Symbols

Symbol	Explanation	Unit
α	Thermal expansion	K^{-1}
γ	Grüneisen parameter	–
γ^*	Pseudocritical exponent	–
δ	Anderson–Grüneisen parameter	–
$\underline{\theta}$	Parameter vector	–
θ_E	Einstein temperature	K
κ	Isothermal compressibility	Pa^{-1}
Λ	Eigenvalue matrix	–
μ	Chemical potential	$J\,mol^{-1}$
χ^2	Chi-squared value	–
A	Helmholtz energy	$J\,mol^{-1}$
a^*	Interatomic spacing	m^3
a, b, c	Coefficients	–
C_p	Isobaric heat capacity	$J\,mol^{-1}\,K^{-1}$
C_V	Isochoric heat capacity	$J\,mol^{-1}\,K^{-1}$
E	Energy	$J\,mol^{-1}$, J
E	Expectency	–
e	Unit vector	–

Continued on next page

Continued from previous page

Symbol	Explanation	Unit
F	Force	N
f	Eulerian strain	–
G	Gibbs energy	$\mathrm{J\,mol^{-1}}$
K	Isothermal bulk modulus	Pa
K'	First order pressure derivative of bulk modulus	–
K''	Second order pressure derivative of bulk modulus	$\mathrm{Pa^{-1}}$
K_S	Isentropic bulk modulus	Pa
k_b	Boltzmans constant	J K
N	Mole number	mol
$\underline{n}$	Mole number	mol
p	Pressure	Pa
Q	Eigenvector matrix	–
R	Universal gasconstant	$\mathrm{J\,mol^{-1}\,K}$
r_{ws}	Wigner–Seitz radius	m
S	Entropy	$\mathrm{J\,mol^{-1}\,K^{-1}}$
T	Temperature	K
U	Internal energy	$\mathrm{J\,mol^{-1}}$
V	Volume	$\mathrm{m^3\,mol^{-1}}, \mathrm{m^3}$

Chapter 1

Introduction

In order to find solutions to a variety of problems in earth science and condensed phase physics, an equation of state (EOS) that accurately predicts solids behaviour at high pressure and temperature is required. A well defined EOS provides the opportunity to calculate a number of thermodynamic properties with the use of limited experimental data.

The most famous EOSs for solids are the Murnaghan and the Birch–Murnaghan equations. Murnaghan presented in 1944 an EOS that was based on the principle of conservation of mass, Hooke's law for infinitesimal variations of stress and an assumption that the bulk modulus was linear with respect to pressure (Murnaghan 1944). This assumption has been proven accurate at low compression by comparison with experimental data (Wedepohl 1976). Murnaghan's EOS is still used today and has also been further developed by extending the approximation for the bulk modulus to higher order Taylor expansion with pressure (Fuchizaki 2006). The second order form has been referred to as the modified Murnaghan equation (Birch 1986). The higher order approximations give more complicated calculations. In addition, it is difficult to experimentally determine the higher order derivatives of the bulk modulus. Today, the second derivative of the bulk modulus define the experimental edge of the penumbra (Anderson 1995). Thus, the most common form is still truncation at the linear term. However, for parameter fitting the modified/second order Murnaghan equation is still useful, as shown in this report.

A derivation based on finite strain theory, which in a simpler way takes into account the variation of the bulk modulus with respect to pressure, was made by Birch (Birch 1947). This equation is popularly refered to as the Birch–Murnaghan EOS.

Both the Murnaghan and the Birch–Murnaghan are isothermal equations, i.e. they are not temperature dependent. To find the temperature dependency of a solid, isobaric EOSs has often been used (Plymate & Stout 1989). The simplest one is just the definition of the thermal expansion:

$$\alpha = -V^{-1}\left(\frac{\partial V}{\partial T}\right)_p \tag{1.0.1}$$

The compression of a solid is for most materials much more dependent on pressure than temperature. Thus, the approach to find the EOS that gives good fit at both high pressure and temperature has been to use a isothermal EOS, and then add a thermal expansion correction (Anderson 1995).

In addition to Murnaghan and Birch–Murnaghan there is a large number of other EOSs which are made for the isothermal description of solids under strong compression. Many of them are similar, and can consequently be lumped into classes which describes the foundation that they are built upon. For instance the Bardeen, Ullman-Pan'kov and Thomsen EOS are all based on the same foundation as the Birch–Murnaghan, i.e. finite strain theory (Anderson 1995). In this report the isothermal EOSs are divided into four main classes given as follows:

1) Based on solid mechanics definition of finite strain.
2) Empirical model for certain state properties, e.g. bulk modulus, K.
3) Based on interatomic potential.
4) The pseudo-spinodal hypothesis.

For each of the four classes an isothermal EOS has been chosen to represent that specific class. The choice of EOS has been based on earlier documentation of their success to fit experimental data. The selected isothermal EOS are given with the same numbering as the class they represent, and are as follows:

1) Birch–Murnaghan
2) Murnaghan
3) Vinet
4) Pseudo-spinodal

This report will focus on the aforementioned isothermal EOSs as well as a suggestion to a complete EOS. Here, the complete EOS is built up from two contributions. The isothermal EOS that gives the best fit to experimental data, and a temperature dependency which is incorporated into that equation.

Chapter 2

Theory

This chapter outlines the background for and the derivation of the EOSs used in this thesis. Also, the basis for a thermodynamic state description has been outlined, i.e. to establish a complete set of equation of states in the Gibbs and Helmholtz framework. The differential of Gibbs potential at constant temperature and pressure is as follows:

$$(\mathrm{d}G)_{T,p} = \sum_i \mu_i \mathrm{d}N_i \tag{2.0.1}$$

The differential of Helmholtz potential at constant temperature is as follows:

$$(\mathrm{d}A)_T = -p\mathrm{d}V + \sum_i \mu_i \mathrm{d}N_i \tag{2.0.2}$$

To be able to integrate Equations 2.0.1 and 2.0.2 it is necessary to know the functions μ_i(T,p,$\underline{\mathrm{n}}$), or p(T,V,$\underline{\mathrm{n}}$) and μ_i(T,V,$\underline{\mathrm{n}}$) respectively. Note the different free variables for the Gibbs and the Helmholtz potentials. Section 2.5 describes how the chemical potential can be found based on integration of V(p) and p(V).

2.1 Physical properties and thermoelastic parameters

Table 2.1.1 gives an overview of the different experimental physical properties, and the thermoelastic parameters that are used in the field of high pressure condensed phase thermodynamics. The parameter names, symbols and meanings in terms of differentials

are stated. The symbols used for the different parameters are chosen in accordance to the IUPAP standard (Mills, Cvitas, Homann, Kallay & Kuchitsu 1993), and alternative names found in the literature are also given in parenthesis.

Table 2.1.1: Overview of thermodynamic state properties with interest to condensed phase high pressure physics and their meaning in terms of differentials. Symbols in paranthesis are alternative names found in litterature.

Parameter name	Symbol	Derivative	Equivalence
Thermal expansion	α	$V^{-1}\left(\frac{\partial V}{\partial T}\right)_p$	
Isothermal bulk modulus	$K, (K_T, B_T, B)$	$-V\left(\frac{\partial p}{\partial V}\right)_T$	
Isothermal compressibility	$\kappa, (\beta)$	$-V^{-1}\left(\frac{\partial V}{\partial p}\right)_T$	
Nameless parameter	αK	$\left(\frac{\partial p}{\partial T}\right)_V$	$-\left(\frac{\partial V}{\partial T}\right)_p\left(\frac{\partial p}{\partial V}\right)_T$
Isochoric heat capacity	C_V	$T\left(\frac{\partial S}{\partial T}\right)_V$	
Isobaric heat capacity	C_p	$T\left(\frac{\partial S}{\partial T}\right)_p$	
Pressure derivative of bulk modulus	K'	$\left(\frac{\partial K}{\partial p}\right)_T$	
Temperature derivative of bulk modulus	$\left(\frac{\partial K}{\partial T}\right)_p$	$\left(\frac{\partial K}{\partial T}\right)_p$	
Anderson–Grüneisen	$\delta, (\delta_T)$	$-\frac{1}{\alpha K}\left(\frac{\partial K}{\partial T}\right)_p$	
Grüneisen	$\gamma, (\gamma^G, \gamma_{mg})$	$V\left(\frac{\partial p}{\partial U}\right)_V$	$\frac{\alpha K V}{C_V}$
Isentropic bulk modulus	K_S	-V$\left(\frac{\partial p}{\partial V}\right)_S$	
Intrinsic temperature derivative of K	$\left(\frac{\partial K}{\partial T}\right)_V$	$\left(\frac{\partial K}{\partial T}\right)_V$	$\left(\frac{\partial K}{\partial T}\right)_p + \alpha K\left(\frac{\partial K}{\partial p}\right)_T$

The differentials in Table 2.1.1 are rewritten in terms of Helmholtz and Gibbs potentials in Table 2.1.2. This is done to represent these parameters as functions of energies. No equivalent setup as the one given in Table 2.1.2 is found in the literature, but some of the energy derivatives are derived in the book by Anderson (1995).

Table 2.1.2: State properties given as energy function derivatives. Gibbs energy is explicit in temperature and pressure, whilst Helmholtz energy is explicit in temperature and volume.

Symbol	Gibbs energy	Helmholtz energy
α	$\frac{1}{V}G_{pT}$	$-\frac{1}{V}\frac{A_{VT}}{A_{VV}}$
K	$-V\frac{1}{G_{pp}}$	VA_{VV}
κ	$-\frac{1}{V}G_{pp}$	$\frac{1}{V}\frac{1}{A_{VV}}$
αK	$-\frac{G_{pT}}{G_{pp}}$	$-A_{VT}$
C_V	$-T(G_{TT}+\frac{G_{pT}^2}{G_{pp}})$	$-TA_{TT}$
C_p	$-TG_{TT}$	$T(-A_{TT}+\frac{A_{VT}^2}{A_{VV}})$
K'	$-(1+\frac{G_{ppp}G_p}{G_{pp}^2})$	$-(1+V\frac{A_{VVV}}{A_{VV}})$
$\left(\frac{\partial K}{\partial T}\right)_p$	$\frac{G_{pT}G_{pp}-G_{ppT}G_p}{G_{pp}^2}$	$VA_{VVT}-A_{VT}(1+V\frac{A_{VVV}}{A_{VV}})$
δ	$-\frac{G_pG_{ppT}}{G_{pT}G_{pp}}-1+\frac{G_pG_{ppp}}{G_{pp}^2}$	$V\frac{A_{VVT}}{A_{VT}}-(1+V\frac{A_{VVV}}{A_{VV}})$
γ	$\frac{V}{T}\frac{G_{pT}}{(G_{TT}G_{pp}+G_{pT}^2)}$	$\frac{V}{T}\frac{A_{VT}}{A_{TT}}$
K_S	$-\frac{V}{G_{pp}}+TV\frac{G_{pT}^2}{G_{pp}^2}$	$VA_{VV}-V\frac{A_{VT}^2}{A_{TT}}$
$\left(\frac{\partial K}{\partial T}\right)_V$	$-\frac{G_{ppT}G_p}{G_{pp}^2}$	VA_{VVT}

2.2 Isothermal equations of state

The four different EOSs studied in this report, i.e. Murnaghan, Birch–Murnaghan, Vinet and the pseudo-spinodal equation, can be classified into either an integral or a derivative form. Birch–Murnaghan and Vinet are both based on the derivative of the internal energy:

$$p = -\left(\frac{\partial U}{\partial V}\right)_{T=0} \tag{2.2.1}$$

Whilst the Murnaghan and Pseudo-spinodal EOS are based on the pressure integral form:

$$\frac{V}{V_0} = \exp\left[-\int_{p_0}^{p} \frac{\mathrm{d}p}{K(p)}\right] \tag{2.2.2}$$

The isothermal EOSs which are used throughout this report are shown in Table 2.2.1 for the pressure explicit form and in Table 2.2.2 for the volume explicit form. The pseudo-spinodal and Murnaghan EOS can be expressed explicitly in both pressure and volume. EOSs which have this feature have been referred to as invertible EOSs (Chauhan, Lal & Singh 2011). In contrast, the Vinet and Birch–Murnaghan EOS are non-invertible and can only be given in pressure.

Table 2.2.1: Isothermal EOSs, pressure explicit

Equation of state	Explicit in pressure
Murnaghan (1st order)	$p(V) = \frac{K_0}{K_0'}\left[\left(\frac{V_0}{V}\right)^{K_0'} - 1\right]$
Birch–Murnaghan (3rd order)	$p(V) = \frac{3}{2}K_0\left(\frac{V}{V_0}\right)^{-\frac{7}{3}}\left(1 - \left(\frac{V}{V_0}\right)^{\frac{2}{3}}\right)\left[1 + \frac{3}{4}(K_0' - 4)\left(\left(\frac{V}{V_0}\right)^{-\frac{2}{3}} - 1\right)\right.$
Vinet	$p(V) = 3K_0\frac{1-\left(\frac{V}{V_0}\right)^{\frac{1}{3}}}{\left(\frac{V}{V_0}\right)^{\frac{2}{3}}}\exp\left[\frac{3}{2}(K_0' - 1)\left(1 - \left(\frac{V}{V_0}\right)^{\frac{1}{3}}\right)\right]$
Pseudo-spinodal	$p(V) = \left[\ln\left(\frac{V}{V_{sp}}\right)\frac{(\gamma^* - 1)}{\kappa^*}\right]^{\frac{1}{(1-\gamma^*)}} + p_{sp}$

Table 2.2.2: Isothermal EOSs, volume explicit

Equation of state	Explicit in volume
Murnaghan	$V(p) = V_0\left(\frac{K_0+K_0'p}{K_0+K_0'p_0}\right)^{-\frac{1}{K_0'}}$
Birch–Murnaghan (3rd order)	Not invertible
Vinet	Not invertible
Pseudo-spinodal	$V(p) = V_{sp}\exp\left(-\frac{\kappa^*}{1-\gamma^*}(p-p_{sp})^{(1-\gamma^*)}\right)$

A fundamental constraint required by any EOS is that when the volume approaches zero, the pressure must increase towards infinity (Chauhan et al. 2011). By inserting $\frac{V}{V_0} \to 0$ in the equations in Table 2.2.1 it can be seen that for all the EOSs investigated here $p \to \infty$ when the volume decreases towards zero. Thus, all the equations exhibit correct high compression asymptotes. However, for the Birch–Murnaghan EOS there is an additional constraint on the parameters for which the potential is physically realistic (Hofmeister 1993). The Birch–Murnaghan is mathematically unstable for $K_0' < 4$. Below this value the bulk modulus will become negative given sufficient compression. This is obvious from the Birch–Murnaghan EOS given in Table 2.2.1. However, the potential is not physically unrealistic before $K_0' \lesssim 3.8$. This is due to the prevention of collapse in the potential, which is a result of the big values for the maxima as K_0' approaches 4 (Hofmeister 1993). For the Birch–Murnaghan EOS, the mathematically stable and physically realistic potential region for ionic solid or soft solids (e.g. NaCl) is $4 < K_0' \lesssim 8$ (Hofmeister 1993). For neutral or hard solids (e.g. MgO), the region is $4 < K_0' \lesssim 6$ (Hofmeister 1993). Most solids lie within this range, and the EOS is therefore usable for solids. For liquids on the other hand, where $K_0' > 7$, the Birch–Murnaghan EOS is unreliable.

Specially designed isothermal EOSs are possible to derive for each substance in question through so-called first principle calculations developed from quantum mechanics. These calculations give more accurate descriptions of the solid, but are very time-consuming as they have to be computed individually for a number of volumes and for each substance class. On the other hand, if a suitable analytical form of the EOS is found, the high pressure and high temperature properties for a variety of substances can be predicted by determining a few parameters by fitting to experimental data.

2.3 Derivations of the isothermal EOSs

The derivations of the isothermal EOSs are shown in the following section.

2.3.1 Murnaghan

Murnaghan's EOS can be derived from the definition of the bulk modulus (see Table 2.1.1) and the assumption made by Murnaghan that the bulk modulus is linear with respect to pressure (Murnaghan 1944):

$$K(p) = K_0 + K_0' P \tag{2.3.1}$$

By insertion of Equation 2.3.1 into the pressure integral in Equation 2.2.2 and carrying out the integration, the following equation is obtained:

$$\left(\frac{V}{V_0}\right) = \left(1 + \frac{K_0'}{K_0} p\right)^{-\frac{1}{K_0'}} \tag{2.3.2}$$

This basic form is the so-called Murnaghan EOS. However, as is widely known in the literature the Murnaghan equation is not valid at large compressions. It starts to break down at compressions below approximately (0.85 – 0.90) $\frac{V}{V_0}$ for most solids (Plymate & Stout 1989) and at even larger compressions Murnaghan's equation starts to deviate significantly from experimental data (Fuchizaki 2006).

2.3.2 Vinet

The Vinet EOS is based on a relationship between the binding energies and the interatomic spacing, given the closed form (Vinet & Ferrante 1987):

$$E(a^*) = \Delta E[E^*(a^*)] \tag{2.3.3}$$

The interatomic separation a^* is defined as:

$$a^* = \frac{(r_{ws} - r_{wse})}{l} \tag{2.3.4}$$

Here, $E(a^*)$ is the binding energy and ΔE is the zero pressure value. r_{ws} is the Wigner–Seitz radius, r_{wse} is the Wigner–Seitz radius at equilibrium and l is a scaling length. The Wigner–Seitz radius is the radius of a sphere, whose volume is the average volume per

atom in the system under consideration. At zero temperature the pressure can be found from (Vinet & Ferrante 1987):

$$p = -\left(\frac{\partial A}{\partial V}\right)_{T=0} = -\left(\frac{\partial E}{\partial V}\right)_{T=0} = \frac{\Delta E}{4\pi(la* + r_{ws})^2}\frac{1}{l}E^{*'}(a^*) \tag{2.3.5}$$

The force relation can then be written as:

$$F(a^*) = 4\pi r_{ws}^2 P(a^*) = \frac{-\Delta E}{l}E^{*'}(a^*) \tag{2.3.6}$$

By employing Hooke's law near equilibrium and the approximation for solids that $E^{*'}(a^*)$ is approximated by $-(1 + a^*)\exp(a^*)$ the final result can be written as:

$$p(V) = 3K_0\frac{1 - (\frac{V}{V_0})^{\frac{1}{3}}}{(\frac{V}{V_0})^{\frac{2}{3}}}\exp\left[\frac{3}{2}(K_0' - 1)(1 - (\frac{V}{V_0})^{\frac{1}{3}})\right] \tag{2.3.7}$$

See Vinet & Ferrante (1987) for details.

2.3.3 Birch–Murnaghan

The Birch–Murnaghan EOS is developed from the internal potential energy in a solid, and as explained earlier based on finite strain theory. The energy of a solid can be expressed by the Helmholtz energy which for most solids has three main contributions (Anderson 1995):

$$A = E_{st} + A_{Vib} + E_{el} \tag{2.3.8}$$

Here, A is the Helmholtz energy, E_{st} is the potential of the static lattice at absolute zero temperature, A_{Vib} is the vibrational energy due to the atoms motion around a lattice point and E_{el} is the potential due to free electrons. There also exists other contributions, e.g. magnetization, but they may be assumed small compared to the other contributions for most solids. For non-conducting materials E_{el} may also be assumed negligible. This theory states that the strain energy of a solid can be found based on a Taylor series expansion of energy with respect to Eulerian strain, which is defined as follows:

$$f = \frac{1}{2}\left[\left(\frac{V_0}{V}\right)^{\frac{2}{3}} - 1\right] \tag{2.3.9}$$

At zero temperature and assuming negligible E_{el}, the energy function can be written as $A \approx E_{st}$. The Helmholtz energy can now be expressed as a Taylor series expansion of the

Eulerian strain:

$$A = a + bf + cf^2 + df^3 + \dots \tag{2.3.10}$$

Truncating Equation 2.3.10 after the second order term and acknowledging that the energy is zero at zero strain, the following is obtained:

$$A = bf + cf^2 \tag{2.3.11}$$

The pressure can then be found from the definition:

$$p = -\left(\frac{\partial A}{\partial V}\right)_T = -\left(\frac{\partial A}{\partial f}\right)\left(\frac{\partial f}{\partial V}\right) \tag{2.3.12}$$

Differentiating the two differentials separately and inserting them in Equation 2.3.12 gives:

$$p = b\frac{(1+2f)^{\frac{5}{3}}}{3V_0} + 2cf\frac{(1+2f)^{\frac{5}{3}}}{3V_0} \tag{2.3.13}$$

At zero strain the pressure is also zero, which gives $b = 0$. By using the definition of the bulk modulus (see Table 2.1.1) the last unknown coefficient, c, can be found.

$$K = -V\left(\frac{\partial p}{\partial V}\right)_T = \frac{2cV}{9V_0}(1+2f)^{\frac{5}{2}}\left[5f(1+2f)^{\frac{3}{2}} + (1+2f)^{\frac{5}{2}}\right] \tag{2.3.14}$$

From evaluation of the bulk modulus at zero strain the following equation for pressure is obtained:

$$p = 3K_0 f(1+2f)^{\frac{5}{2}} \tag{2.3.15}$$

By inserting the definition of the Eulerian strain from Equation 2.3.9, the second order Birch–Murnaghan EOS is found:

$$p = \frac{3}{2}K_0\left(\left(\frac{V}{V_0}\right)^{-\frac{7}{3}} - \left(\frac{V}{V_0}\right)^{-\frac{5}{3}}\right) \tag{2.3.16}$$

A similar derivation as the one given above, but now truncating after the third order term in Equation 2.3.10, will give the third order Birch–Murnaghan EOS as shown in Equation 2.3.17 (Anderson 1995).

$$p = \frac{3}{2}K_0\left(\left(\frac{V}{V_0}\right)^{-\frac{7}{3}} - \left(\frac{V}{V_0}\right)^{-\frac{5}{3}}\right)\left[1 + \frac{3}{4}(K_0' - 4)\left(\left(\frac{V}{V_0}\right)^{-2} - 1\right)\right] \tag{2.3.17}$$

2.3.4 Pseudo-spinodal

The pseudo-spinodal EOS is based on the assumption that the bulk modulus, K, follows a power law of the form (Baonza, Alonso & Nunez 1994):

$$K = \frac{1}{\kappa^*}(p - p_{sp})^{\gamma^*} \tag{2.3.18}$$

Here, p_{sp} is the spinodal pressure, κ^* is an amplitude and γ^* is the pseudocritical exponent which characterize the pressure behaviour of the bulk modulus. The spinodal pressure can be considered as the negative hydrostatic pressure at which the solid ruptures (Taravillo, Baonza, Rubio, Nunez & Caceres 2001). The pseudocritical exponent is assumed to be approximately 0.85 for solids (Taravillo et al. 2001). This assumption derives from an analysis, which showed that the Helmholtz energy could be expressed as a Taylor series expansion in $V - V_{sp}(T)$ (Speedy 1982). Here, V_{sp} is the volume of the substance at the cross-section between the isotherm and the spinodal curve. The requirement is that the Helmholtz energy must be analytically near the spinodal. Through this analysis the following was obtained along any isotherm:

$$K \propto \alpha^{-1} \propto C_v^{-1} \propto (|p - p_{sp}(T)|)^{\gamma^*} \tag{2.3.19}$$

Combining the definition of K as given in Table 2.1.1 and Equation 2.3.18, the following can be found:

$$\int_{V_{sp}}^{V} \mathrm{d}\ln V = -\int_{p_{sp}}^{p} \frac{\kappa^*}{1-\gamma^*}[(p - p_{sp})^{1-\gamma^*}]\mathrm{d}p \tag{2.3.20}$$

Integration of Equation 2.3.20, the following equation is found:

$$V(p) = V_{sp}\exp\Big[-\frac{\kappa^*}{(1-\gamma^*)}(p - p_{sp})^{1-\gamma^*}\Big] \tag{2.3.21}$$

where,

$$p_{sp} = \frac{-\gamma^* K_0}{K_0'} \tag{2.3.22}$$

$$\kappa^* = \frac{(-p_{sp})^{\gamma^*}}{K_0} \tag{2.3.23}$$

$$\frac{V_{sp}}{V_0} = \exp\Big[\frac{\gamma^*}{(1-\gamma^*)K_0'}\Big] \tag{2.3.24}$$

Equation 2.3.21 is the so-called pseudo-spinodal EOS. It may seem like there is a unit inconsistency since the pressure difference $(p - p_{sp})$ has a non integer power. However, by

rewriting Equation 2.3.21 it is evident that the dimensions are consistent:

$$V(p) = V_{sp} \exp\Big[\frac{(1-\frac{p}{p_{sp}})^{-\gamma^*}(p_{sp}-p)}{(1-\gamma^*)K_0}\Big] \tag{2.3.25}$$

2.4 Incorporation of thermal effects

In order to find a complete EOS with both pressure and temperature dependency the total differential of pressure can be used.

$$\mathrm{d}p(V,T) = \left(\frac{\partial p}{\partial V}\right)_T \mathrm{d}V + \left(\frac{\partial p}{\partial T}\right)_V \mathrm{d}T \tag{2.4.1}$$

Inserting the definition of αK (see Table 2.1.1) in Equation 2.4.1 the following is obtained:

$$\mathrm{d}p(V,T) = \left(\frac{\partial p}{\partial V}\right)_T \mathrm{d}V + \alpha K \mathrm{d}T \tag{2.4.2}$$

Assuming that the volume term is independent of temperature and the temperature term is independent of volume, the equation can be integrated as follows:

$$p(V,T) = \int_{V_0}^{V} \left(\frac{\partial p}{\partial V}\right)_T \mathrm{d}V + \int_{T_0}^{T} \alpha K \mathrm{d}T + p(V_0,T_0) \tag{2.4.3}$$

If αK is assumed to be constant with respect to temperature, which is shown to be approximately true for a variety of substances above the Debye temperature, the following EOS is obtained:

$$p(V,T) = \int_{V_0}^{V} \left(\frac{\partial p}{\partial V}\right)_T \mathrm{d}V + \alpha K(T-T_0) + p(V_0,T_0) \tag{2.4.4}$$

By carrying out the integration of Equation 2.4.4 the final equation can be written as:

$$p(V,T) = p(V,T_0) + \alpha K(T-T_0) \tag{2.4.5}$$

Here, $p(V,T_0)$ can be replaced by any one of the isothermal equations given in Table 2.2.1.

This procedure of including pressure and temperature effects separately was used by Anderson (1995). In his work a general EOS was defined as follows:

$$p(V,T) = p(V,T_0) + p_{th}(V,T) \tag{2.4.6}$$

Here, $p(V, T_0)$ is the isothermal contribution at T_0 and p_{th} is the thermal pressure. The thermal pressure can be found through the Mie–Grüneisen approximation (Anderson 1995):

$$p_{th} = \frac{\gamma_{mg}}{V} E_{th} \tag{2.4.7}$$

Here, γ_{mg} is the Mie–Grüneisen parameter, an approximation of the Grüneisen parameter (γ, see Table 2.1.1), and E_{th} is the thermal energy.

The thermal energy in solids can be viewed as an analog to the internal energy in gases. The internal energy of a perfect gas can be written as:

$$U = C_v T \tag{2.4.8}$$

From ideal gas law the following can be obtained:

$$\frac{T}{V} = \frac{p}{NR} \tag{2.4.9}$$

By combining Equation 2.4.8 and Equation 2.4.9 the following relation can be found:

$$p^{ig} = \frac{R}{C_V} \frac{U}{V} \tag{2.4.10}$$

A comparison of Equation 2.4.10 with Equation 2.4.7 shows that they are analogous except for the proportional constant, which is different. Also, the thermal pressure in a solid is only a part of the total pressure, whilst for gases the kinetic pressure equals the total pressure.

The thermal energy, E_{th}, in Equation 2.4.7 can be found from either Einstein's or Debye's model. Einstein's model assume that all the particles in the lattice vibrates with the same frequency. Debye's model takes into account that the frequency can be different for each individual particle (Haug-Warberg 2006).

Another method of including the temperature effect is due to Vinet et al. (1986). They included the temperature effect into their EOS by modelling the variation of bulk modulus with temperature (Vinet, Smith, Ferrante & Rose 1986). To include this effect experimental values of the thermal expansion, V_0, K_0 and K_0' are needed at zero pressure and at a single reference temperature. In this EOS the thermal pressure was assumed independent of volume and linear with temperature above the Debye temperature ($T > \theta$). Thus, the Vinet EOS is only applicable above the Debye temperature (Taravillo et al. 2001), while the pseudo-spinodal theory is also valid at lower temperatures.

A third alternative was proposed by Taravillo et al. (2001). They used the same Mie–Grüneisen approximation as in Equation 2.4.7, but in a slightly different manner. Instead of using the Mie–Grüneisen approximation to find the thermal pressure, they used it to find the pseudo-spinodal pressure (Taravillo et al. 2001):

$$p_{sp}(T) = p_{sp}^0 + \frac{\gamma_0}{V_0} E_{th}(T) \tag{2.4.11}$$

As described above both Einstein's and Debye's model can be used to find E_{th}. In the pseudo-spinodal EOS the Einstein model was chosen since no significant improvement was found by using the Debye model (Baonza, Taravillo, Caceres & Nunez 1995). Besides, the Debye C_V can not be integrated analytically. This gives:

$$p_{sp}(T) = p_{sp}^0 + \frac{\gamma_0}{V_0} 3Nk_b\theta_E\left[\frac{1}{2} + \frac{1}{\exp\frac{\theta_E}{T} - 1}\right] \tag{2.4.12}$$

Here, the p_{sp}^0 is given as the rupture pressure at 0 K. This pressure can be viewed as an offset on the left side of Equation 2.4.12. It is calculated from Equation 2.4.12 if $p_{sp}(T)$ is found at a reference temperature (typically ambient temperature) and the rest of the parameters in the equation is known. The $p_{sp}(T_{ref})$ is calculated from Equation 2.3.22 with the parameters found at that particular reference temperature (Baonza 2012). Then p_{sp}^0 is the only unknown in Equation 2.4.12 and can therefore be solved for:

$$p_{sp}^0 = p_{sp}(T_{ref}) - \frac{\gamma_0}{V_0} 3Nk_b\theta_E\left[\frac{1}{2} + \frac{1}{\exp\frac{\theta_E}{T_{ref}} - 1}\right] \tag{2.4.13}$$

By using the latter approach to introduce the thermal effects some of the problems concerning the volume dependency of the ratio $\frac{\gamma}{V}$ can be avoided (Taravillo et al. 2001). A lengthy discussion on how this ratio varies with pressure has been done by other authors (Anderson 1995). Nonetheless, there are some problems with an inconsistency in the pseudo-spinodal EOS which will be addressed in Chapter 5.3.

2.5 Derivation of chemical potential

The following section will outline the chemical potential of the aforementioned EOSs. In order to find the chemical potential, a differential based on either Gibbs or Helmholtz variables can be integrated. With Gibbs canonical variables the differential must be

expressed as follows:

$$(\mathrm{d}\mu)_{T,N} = v\mathrm{d}p \tag{2.5.1}$$

In Helmholtz variables the differential is as follows:

$$(\mathrm{d}\mu)_{T,N} = p\mathrm{d}v \tag{2.5.2}$$

Which set of canonical variables one should use depends on what form the EOS can be represented analytically (see Tables 2.2.1 and 2.2.2), either as p(V) or V(p) functions. The chemical potentials from the different EOSs are shown in Table 2.5.1.

Table 2.5.1: Chemical potential for the different EOSs

EOS	Chemical potential
Murnaghan (Gibbs)	$\mu^{Mur}(T,p) = \mu(T,p_0) + V_0\left(\frac{K_0+K_0'p_0}{K_0'-1}\right)\left[\left(\frac{K_0+K_0'p}{K_0+K_0'p_0}\right)^{\left(\frac{K_0'-1}{K_0'}\right)} - 1\right]$
Murnaghan (Helmholtz)	$\mu^{Mur}(T,V) = \mu(T,V_0) + \frac{K_0}{K_0'}\left(V\left(\frac{V}{V_0}\right)^{-K_0'} + K_0'(V-V_0) - V\right)/(1-K_0')$
Birch–Murnaghan	$\mu^{B-M}(T,V) = \mu(T,V_0) - \frac{9}{2}K_0V_0\left[\frac{1}{8}(K_0'-4)\left(\frac{V}{V_0}\right)^{-2} + \left(\frac{7}{4} - \frac{3}{8}K_0'\right)\left(\frac{V}{V_0}\right)^{-\frac{4}{3}} + \left(2 - \frac{3}{8}K_0'\right)\left(\frac{V}{V_0}\right)^{-\frac{2}{3}} + \left(\frac{49}{12} - \frac{5}{6}K_0'\right)\right]$
Vinet	$\mu^{Vin}(T,V) = \mu(T,V_0) + 9K_0V_0\left[-\frac{2}{3(K_0'-1)}\exp\left[\frac{3}{2}(K_0'-1)\left(1-\left(\frac{V}{V_0}\right)^{\frac{1}{3}}\right)\right]\left(1-\left(\frac{V}{V_0}\right)^{\frac{1}{3}}\right) + \frac{4}{9(K_0'-1)^2}\exp\left[\frac{3}{2}(K_0'-1)\left(1-\left(\frac{V}{V_0}\right)^{\frac{1}{3}}\right)\right] - \frac{4}{9(K_0'-1)^2}\right]$
Pseudo-spinodal (Gibbs)	$\mu^{ps}(T,p) = \mu(T,p_0) + V_{sp}\left[\left(p - p_{sp}\left(\frac{\kappa^*}{1-\gamma^*}(p-p_{sp})^{(1-\gamma^*)}\right)^{\left(\frac{1}{\gamma^*-1}\right)}\right)\right] \cdot \Gamma\left(\frac{\kappa^*}{1-\gamma^*}(p-p_{sp})^{(1-\gamma^*)}, \frac{1}{1-\gamma^*}\right)$
Pseudo-spinodal (Helmholtz)	$\mu^{ps}(T,V) = \mu(T,V_0) + V_{sp} - \ln\left(\frac{V}{V_{sp}}\right)^{\frac{1}{\gamma^*-1}}\left(\frac{\gamma^*-1}{\kappa^*}\ln\frac{V}{V_{sp}}\right)^{\frac{1}{1-\gamma^*}}\Gamma\left(-\ln\left(\frac{V}{V_{sp}}\right), \frac{2-\gamma^*}{1-\gamma^*}\right) + p_{sp}V$

[1] $\Gamma(X,a)$ is the incomplete gamma function (Rottmann 2006)

2.6 Statistics

In order to find the standard deviation for the parameters, two different statistical methods have been employed in this study. The first is a statistical method called bootstrapping. This method was developed by Bradley Efron and Robert Tibshirani in the early 1980s (Efron & Tibshirani 1993). This method uses a large number of so-called bootstrap samples to find the accuracy of sample estimates, e.g. in this case, the standard deviation of the parameters. A bootstrap sample is made by taking random samples with replacement from the original data set. It is important that the size of the samples are equal to the size of the original. The covariance matrix can then be obtained through an analysis of the optimal parameters obtained from nonlinear regression of each bootstrap sample. Each element in the covariance matrix can be calculated from (Walpole, Myers, Myers & Ye 2007):

$$cov(\theta_i, \theta_j) = E[(\theta_i - E(\theta_i))(\theta_j - E(\theta_j))] = E[(\theta_i - \hat{\theta}_i)(\theta_j - \hat{\theta}_j)] \tag{2.6.1}$$

The other method utilized is based on maximum likelihood. The covariance matrix is then calculated from the inverse of the Hessian matrix of the implicit parameter fitting equation (Golder n.d.). The Hessian is found by second order differentiation of the likelihood function. This differentiation can be done analytically or numerically. For systems with many unknown parameters and complicated analytical differentials it can be beneficial to do the differentiation numerically.

From the covariance matrix found from either of these statistical methods it is possible to find the variance and consequently the standard deviation of the parameters. If the parameters are correlated it is possible to decorrelate them by changing the coordinate system so that the variance of the parameters are orthogonal on each other. Decorrelation is taken to mean that the variables are scaled and rotated such that the contours becomes concentric circles.

Schematic overviews of how the bootstrap and the maximum likelihood method can be used to find the standard deviation for the parameters are illustrated in Figures 2.6.1 and 2.6.2 respectively.

Bootstrap →

Covariance matrix →

Diagonalization →

Variance →

Standard deviation

Figure 2.6.1: Schematic overview of the bootstrap method for finding the standard deviation of the parameters

Maximum likelihood →

Hessian →

Covariance matrix →

Diagonalization →

Variance →

Standard deviation

Figure 2.6.2: Schematic overview of the maximum likelihood method for finding the standard deviation of the parameters

Chapter 3

Literature study

In order to find optimal parameters for the isothermal EOSs and other characteristic properties, a search for experimental data was required. Pressure-volume relations at constant temperature have been measured for all the substances evaluated in this report to greater or lesser extent. The search tools utilized were Google Scholar, ISI web of knowledge and the library resources available at NTNU.

Isothermal data has been the primary objective, and therefore the available shock data has not been evaluated and used in a systematic way here. One large shock hugoniot database (Marsh 1980) has been used for some of the substances, but the data has subsequently been adjusted to the specific heat ratio. This is only an approximation and it does not give large differences in the parameter fitting if this dataset is left out. It is only used to represent the high pressure range for some of the solids evaluated. The experimental data used in this report has been reprinted in Appendix A.

For MgO a lot of different sources of experimental data were available. Six different sources of data were used containing a total of 218 data points. A lot of low pressure data which matched each other well and some high pressure data that deviated from each other was found for MgO. This gave a high confidence in the low pressure data and low confidence in the high pressure data for this solid. This affected the distribution function as will be discussed in Section 5.4.

Experimental data for CaO was found through five different sources at a total of 58 data points. The experimental measurements for CaO were found to give very similar results

compared to each other as can be seen by comparing the different measurements at similar pressure.

Al_2O_3 had a lot of experimental data available for a wide range of compression. From six different sources a total of 100 experimental measurements were found. The maximum pressure for which measurements were found was at 144.8 GPa.

SiO_2 was a solid for which it was difficult to obtain experimental data. Only 36 data points were found from four different sources. There are a lot more measurements on SiO_2 available, but then for other phases than the one studied here, i.e. α-quartz.

Experimental data for NaCl was found through five different sources. This gave a total of 113 data points. The maximum pressure for which measurements were found was at 33.27 GPa. Since NaCl is a quite soft solid compared to many of the others studied here this pressure gave a compression of $\frac{V}{V_0} = 0.62$. Thus, the pressure is measured high enough to give good data for parameter fitting even though the pressure is not as high as for many of the others.

For $MgCO_3$ only two references for experimental isothermal compression data were found. Nonetheless, one of the databases (Fiquet & Reynard 1999) was extensive enough to provide a total of 66 data points for this solid.

Chapter 4

Results

In this chapter, the results of the model fitting will be outlined. Matlab was used to conduct the calculations and make the plots. A selection of scripts are listed in Appendix B, while the rest can be found in the attached zip file. The selection is done such that scripts with identical functionality, and which differ only in what solids they handle, are listed just once.

4.1 Parameter fitting

In order to find the parameters for the isothermal EOSs, i.e. K_0, K_0', K_0'', a second order Murnaghan EOS on implicit form was used. This equation was used since it is a extension of the Taylor series expansion utilized to calculate the first order Murnaghan EOS.

$$K = \underbrace{\overbrace{K_0 + K_0' p}^{1^{st} order} + \frac{K_0''}{2} p^2}_{2^{nd} order} + \mathcal{O}(p^3) \tag{4.1.1}$$

Since K_0'' is at the limit of what is experimentally measurable there is no reason for extending the Taylor series expansion in Equation 4.1.1 higher than second order. Also, there is found no evidence that this equation is not good enough to fit experimental data. The fact that the equation is written on implicit form means that it is written as $f(p, \frac{V}{V_0}, \underline{\theta}) = 0$, where p is the pressure, $(\frac{V}{V_0})$ is the compression and $\underline{\theta}$ is a vector consisting of the unknown parameters. The equation was derived by integrating the second order bulk

modulus analogous to the derivation of the first order Murnaghan as given in Section 2.3.1. The equation can be written as:

$$\log\left(\frac{V}{V_0}\right) + \frac{1}{K_0(a-b)} \log\frac{(1+ap)}{(1+bp)} = 0 \tag{4.1.2}$$

where,

$$a = \frac{K_0'}{2K_0}\left(1 + \sqrt{\frac{(1-4K_0''K_0)}{K_0''^2}}\right)$$

and

$$b = \frac{K_0'}{K_0} - a$$

The equation is nonlinear in the parameters, and consequently nonlinear regression had to be used to find the optimum. The experimental data for the pressure and the compression were found in the literature (see Appendix A). In Table 4.1.1 the parameters found from the nonlinear regression for the different substances investigated are shown together with their standard deviation. In this table, $\underline{\hat{\theta}}$ is a vector consisting of the optimal isothermal bulk modulus values found from the parameter fitting, i.e. K_0, K_0' and K_0''. The $\Delta\underline{\theta_i}$ vectors are the uncertainty vectors found from the bootstrap method after diagonalization of the covariance matrix. This is explained in Section 2.6.

Table 4.1.1: Nonlinear regression values for the parameters and their uncertainties as given by the bootstrap method. There are three different uncertainty vectors since it is calculated from a covariance matrix.

Substance	$\hat{\underline{\theta}}$	$\pm\Delta\underline{\theta}_1$	$\pm\Delta\underline{\theta}_2$	$\pm\Delta\underline{\theta}_3$	Units
MgO	160	0.000001	0.008561	-2.421412	GPa
	3.9	0.000021	0.076362	0.371368	-
	−0.003	0.000802	-0.002009	-0.003795	GPa^{-1}
CaO	109.4	-4.898921	0.026185	0.000002	GPa
	4.9	0.702416	0.182513	0.000030	-
	−0.028	-0.013587	-0.005618	0.000988	GPa^{-1}
Al_2O_3 (corundum)	270	1E-9	0.009872	-9.097483	GPa
	4.4	0.000012	0.154277	0.582079	-
	−0.013	0.000784	-0.002390	-0.005196	GPa^{-1}
SiO_2(α-quartz)	39	0.000913	0.214945	-2.995555	GPa
	6.0	0.003420	0.376384	1.685451	-
	−0.2	0.021745	-0.068223	-0.139257	GPa^{-1}
NaCl	24.4	0.000025	0.035737	-0.896211	GPa
	5.0	0.000157	0.086438	0.369168	-
	−0.05	0.002096	-0.006905	-0.017092	GPa^{-1}
$MgCO_3$	112	0.000043	0.115360	-3.049675	GPa
	4.8	0.000440	0.429741	0.816764	-
	−0.02	0.007388	-0.026252	-0.030929	GPa^{-1}

The parameters given in Table 4.1.1 are strongly correlated. This can be seen from contour plots made for the different variables. In Figure 4.1.1 a contour plot for MgO is used to show the relation between K_0' and K_0'' at fixed K_0 as an example of the parameters correlation. It is just an illustration. The skewness of the ellipses can of course be changed by simply rescaling the axis. The point is that the ellipses are skewed and that they are not circles.

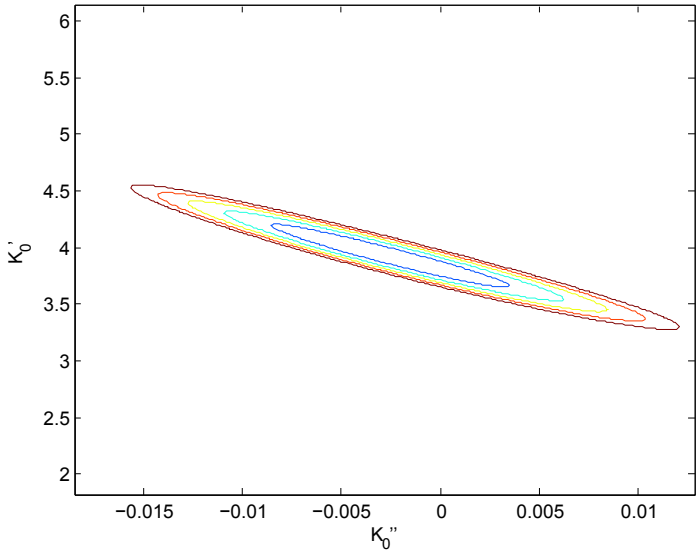

Figure 4.1.1: Contour plot for K_0' versus K_0'' with K_0 constant for MgO

Because of this correlation the covariance matrix between the variables had to be found and evaluated. From diagonalization of the covariance matrix based on an eigenvalue analysis, as described in Section 2.6, the uncorrelated uncertainty vectors were found and given in Table 4.1.1.

4.2 Deviation plots

In order to test the validation of the isothermal EOSs, the bulk modulus for each of them was calculated as $-V\left(\frac{\partial P^{model}}{\partial V}\right)$. Expressions for bulk modulus for the different EOSs are shown in Table 4.2.1.

Table 4.2.1: Bulk modulus for the different EOSs

Equation of state	K
Murnaghan	$K_0(\frac{V}{V_0})^{-K_0'}$
Birch–Murnaghan	$\frac{1}{2}K_0(7(\frac{V}{V_0})^{-\frac{7}{3}} - 5(\frac{V}{V_0})^{-\frac{5}{3}})$ $+\frac{3}{8}K_0(K_0' - 4)(9(\frac{V}{V_0})^{-\frac{9}{3}} - 14(\frac{V}{V_0})^{-\frac{7}{3}} + 5(\frac{V}{V_0})^{-\frac{5}{3}})$
Vinet	$K_0(\frac{V}{V_0})^{-\frac{2}{3}}(1 + (\frac{3}{2}(K_0' - 1)(\frac{V}{V_0})^{\frac{1}{3}} + 1)(1 - (\frac{V}{V_0})^{\frac{1}{3}}))$ $\cdot \exp(\frac{3}{2}(K_0' - 1)(1 - (\frac{V}{V_0})^{\frac{1}{3}}))$
Pseudo-spinodal	$\frac{K_0}{(\gamma^* \frac{K_0}{K_0'})^{\gamma^*}}[\frac{\gamma^* \frac{K_0}{K_0'} - K_0(1-\gamma^*)\ln(\frac{V}{V_0})}{(\gamma^* \frac{K_0}{K_0'})^{\gamma^*}}]^{(\frac{\gamma^*}{1-\gamma^*})}$

A deviation plot from the first order Murnaghan bulk modulus was then plotted for each of the EOSs bulk modulus with the parameter values found from the nonlinear regression explained in Section 4.1. The first order Murnaghan equation serves as a reference equation giving zero deviation. The second order Murnaghan was also plotted with its standard deviation to compare the accuracy of the different EOSs. It is important to emphasize that the shaded area in the deviation plots represent the total uncertainty based on the three different uncertainty vectors given in Table 4.1.1 after being patched together.

The plot of the deviation of bulk modulus versus pressure for MgO is shown in Figure 4.2.1. Then follows CaO, Al_2O_3, SiO_2, NaCl and $MgCO_3$ in Figures 4.2.3 through 4.2.6 respectively.

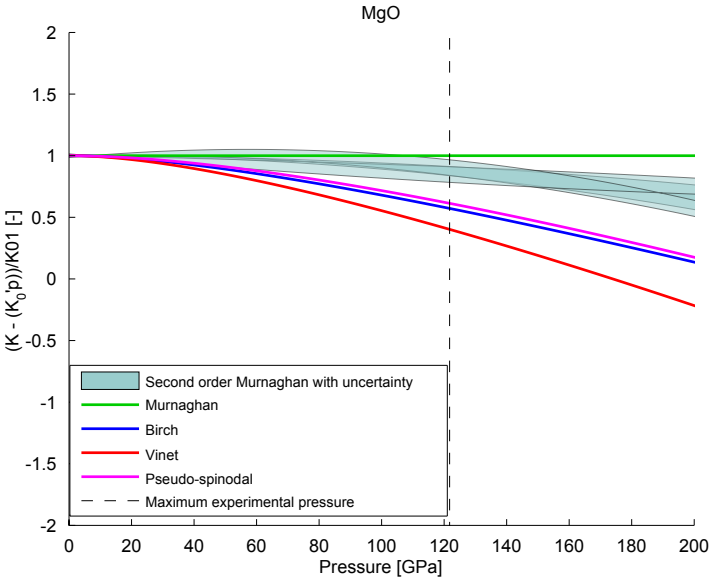

Figure 4.2.1: Deviation plot of bulk modulus for MgO for different EOSs

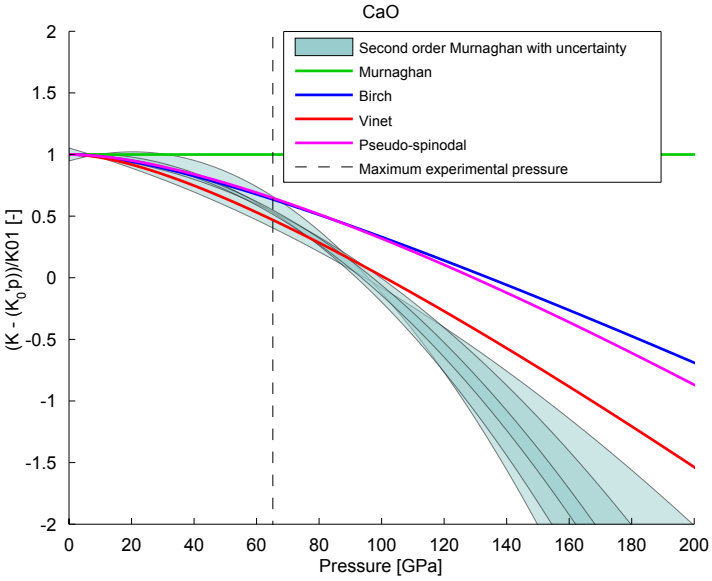

Figure 4.2.2: Deviation plot of bulk modulus for CaO for different EOSs

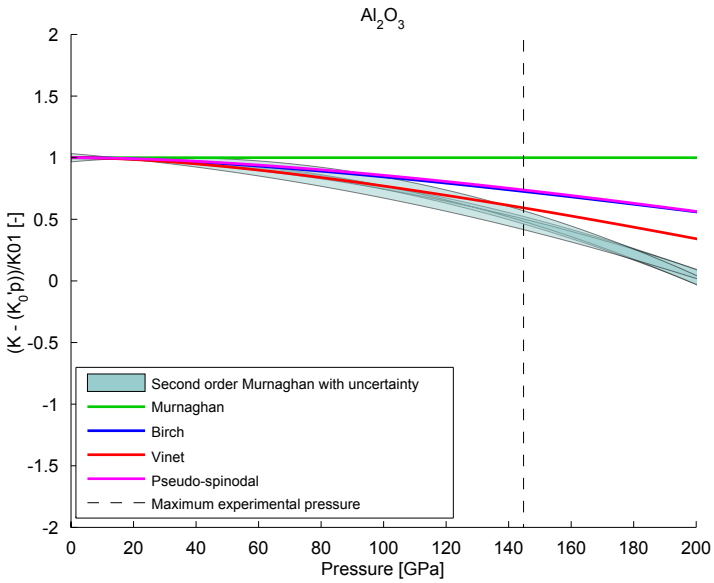

Figure 4.2.3: Deviation plot of bulk modulus for Al_2O_3 for different EOSs

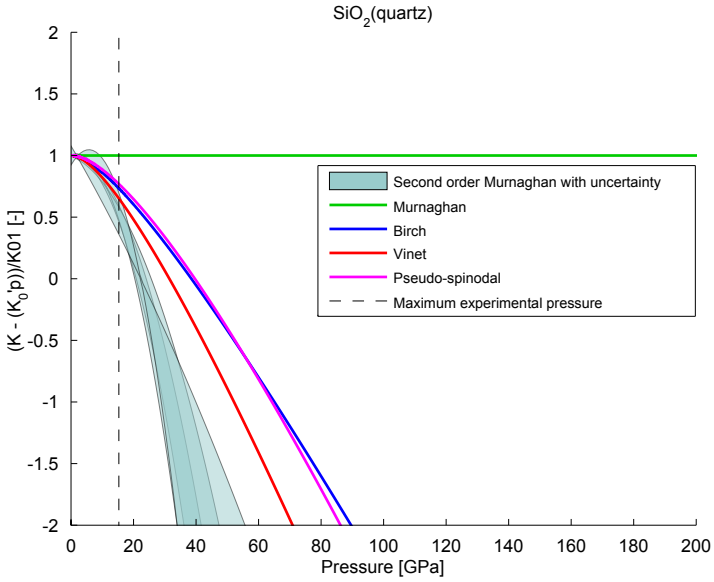

Figure 4.2.4: Deviation plot of bulk modulus for SiO_2 for different EOSs

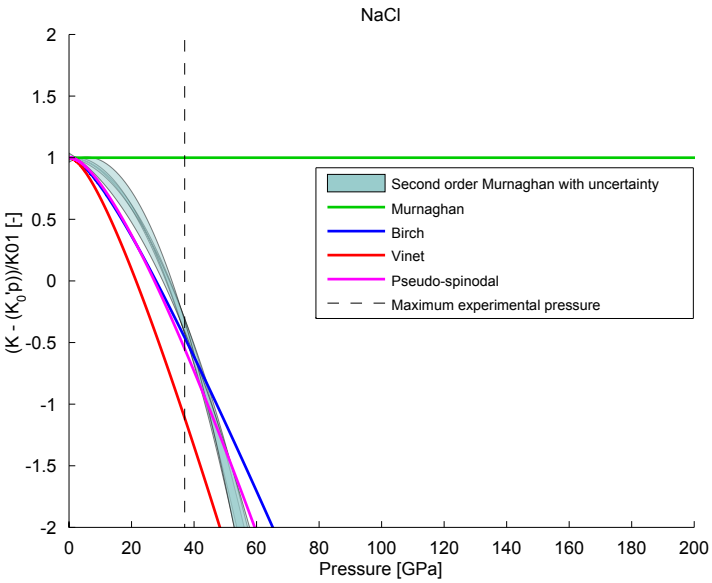

Figure 4.2.5: Deviation plot of bulk modulus for NaCl for different EOSs

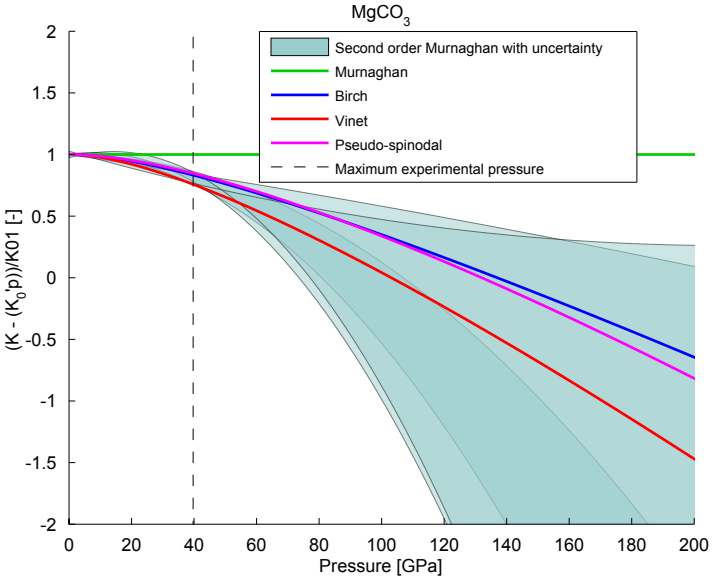

Figure 4.2.6: Deviation plot of bulk modulus for $MgCO_3$ for different EOSs

4.3 Predictions at high temperature and pressure

There is a limited number of substances that have been tested experimentally at both high pressure and temperature. Sodium chloride (NaCl) and magnesium oxide (MgO) are two examples for which data at these conditions can be found. Since the two substances differ from each other significantly when subjected to high pressure, due to the large difference in the value for the bulk modulus (see Table 4.1.1), a wider range of applicability is possible to test than if they had the same properties. However, for a complete understanding of all classes of solids (Silica minerals, oxides, carbonates, halides etc.), an evaluation of a much larger number of substances is required. At least one solid for each class of solid should be tested. This can be done by the methods used here if experimental data is available.

The evaluation of the isothermal equations in Section 2.2 did not provide unambiguous results for which EOS to be used as a complete EOS. A complete EOS is defined here as an isothermal EOS with a temperature dependency incorporated into it. Thus, the choice of a complete EOS was based on the different equations properties as discussed in Section 5.2. The complete EOS used in this evaluation for high pressure and temperature predictions is therefore the isothermal pseudo-spinodal EOS expanded with a thermal contribution. The thermal contribution is based on the Mie–Grüneisen approximation (see Equation 2.4.7).

The parameters needed for the evaluation of the complete pseudo-spinodal EOS are K_0 and K_0' from the present evaluation, and V_0, θ_D and γ_0 from the literature. K_0 and K_0' have been found through the parameter fitting procedure and are given in Table 4.1.1 as well as reprinted in Table 4.3.1. In Table 4.3.1, the extra data from the literature necessary to compute the complete EOS are also given. All the input data must be evaluated at the same reference temperature.

Table 4.3.1: Input parameters for the complete pseudo-spinodal EOS, references are given as superscript

Solid	T_{ref}[K]	$\gamma_0[-]$	$V_0[\frac{\text{cm}^3}{\text{mol}}]$	θ_E[K]	$K_0[-]$	K_0'[GPa^{-1}]
NaCl	298	1.59 [1]	27.0 [1]	241 [1]	160 [5]	3.9 [5]
MgO	298	1.52 [2]	11.25 [3]	743 [4]	24.4 [5]	5.0 [5]

[1] (Taravillo et al. 2001)
[2] (Kushwah & Sharma 2012)
[3] (Mao & Bell 1979)
[4] (Barron, Berg & Morrison 1959)
[5] This study

The pseudo-spinodal EOS was used to predict the high pressure and high temperature behaviour of three important physical parameters, i.e. the isobaric heat capacity (C_p), the thermal expansion (α) and the isothermal compressibility (K). These properties were chosen due to their familiarity with physical chemistry (i.e. in Bridgman tables). The isobaric heat capacity as a function of temperature and pressure for MgO are shown in Figures 4.3.1a and 4.3.1b respectively.

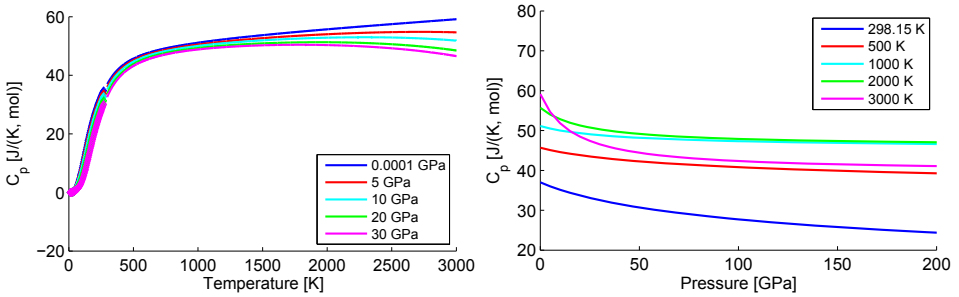

(a) (b)

Figure 4.3.1: Heat capacity, C_p, as a function of temperature (a) and pressure (b) for MgO. Below 298.15 K the curves are based on standard heat capacity from experimental data points (Barron et al. 1959). Above, they are based on a curve fitted function (Chase 1998)

The thermal expansion was calculated based on the pseudo-spinodal EOS as $\alpha(T,p) = \frac{1}{K(T,p)}\left(\frac{\mathrm{d}\,p_{sp}(T)}{\mathrm{d}\,T}\right)$. The thermal expansion as a function of temperature and pressure for MgO are shown in Figures 4.3.2a and 4.3.2b respectively.

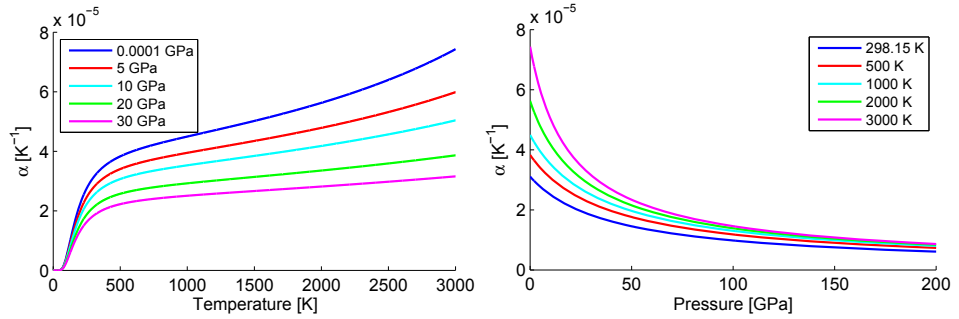

(a) (b)

Figure 4.3.2: Thermal expansion, α, as a function of temperature (a) and pressure (b) for MgO

The isothermal bulk modulus as a function of temperature and pressure for MgO are shown in Figures 4.3.3a and 4.3.3b respectively. The bulk modulus are calculated from Equation 2.3.18.

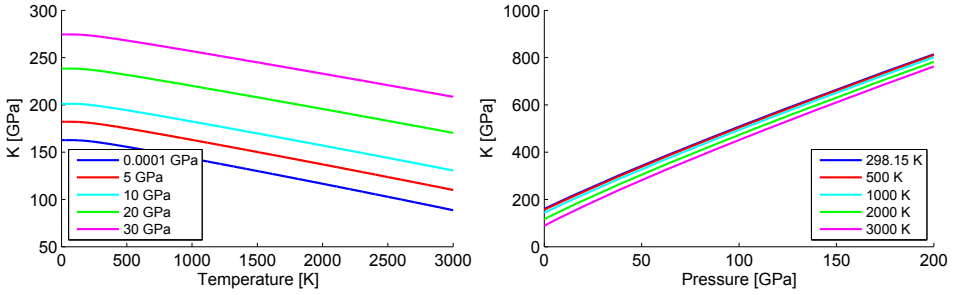

(a) (b)

Figure 4.3.3: Bulk modulus, K, as a function of temperature (a) and pressure (b) for MgO

The isobaric heat capacity as a function of temperature and pressure for NaCl are shown in Figures 4.3.4a and 4.3.4b respectively.

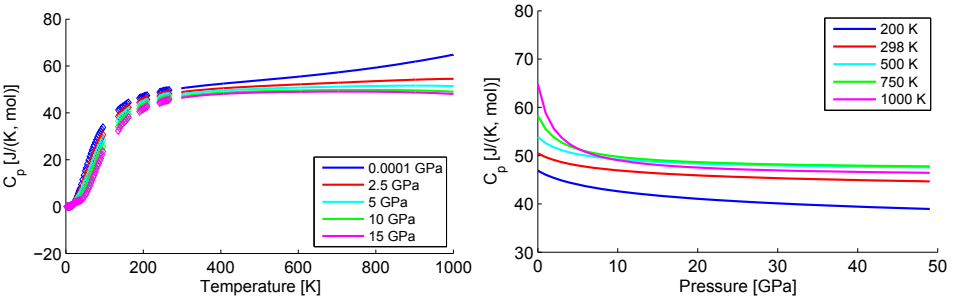

(a) (b)

Figure 4.3.4: Heat capacity, C_p, as a function of temperature (a) and pressure (b) for NaCl. Below 298.15 K the curves are based on standard heat capacity from experimental data points (Barron et al. 1964). Above, they are based on a curve fitted function (Chase 1998)

The thermal expansion as a function of temperature and pressure for NaCl are shown in Figures 4.3.5a and 4.3.5b respectively.

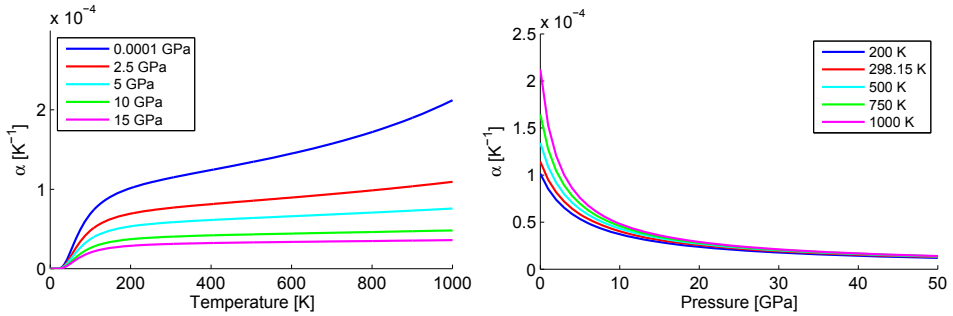

(a) (b)

Figure 4.3.5: Thermal expansion, α, as a function of temperature (a) and pressure (b) for NaCl

The isothermal bulk modulus as a function of temperature and pressure for NaCl are shown in Figures 4.3.6a and 4.3.6b respectively.

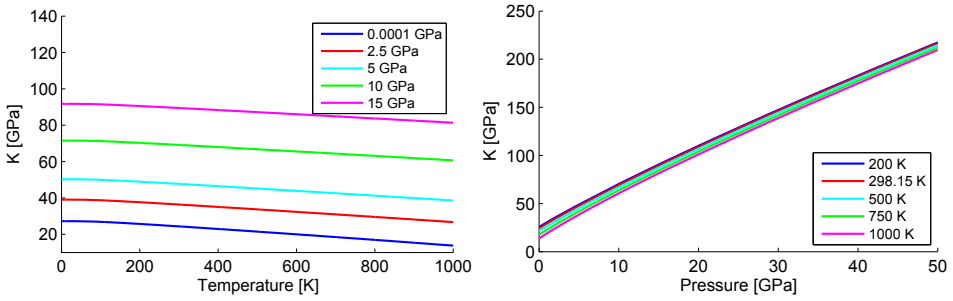

(a) (b)

Figure 4.3.6: Bulk modulus, K, as a function of temperature (a) and pressure (b) for NaCl

The heat capacity for the solids was calculated based on a second order differentiation of the chemical potential with respect to temperature ($Cp = -T\left(\frac{\partial^2 \mu}{\partial T^2}\right)$, see Table 2.1.2). The chemical potential was found from the pseudo-spinodal EOS as shown in Table 2.5.1. The heat capacity at standard conditions is reported as curve fitted functions based on experimental data for temperatures above 298.15 K (Chase 1998). Below 298.15 K the standard heat capacity is given as from experimental data points for MgO (Barron et al. 1959) and NaCl (Barron et al. 1964). Thus, the plots of heat capacity are constructed from points below 298.15 K and continues lines above 298.15 K. The plots show the

sum of the standard heat capacity and the calculated heat capacity contribution from the pseudo-spinodal EOS:

$$C_p(T,p) = C_p^0(T,p_0) + \Delta C_p(T,p) \tag{4.3.1}$$

Chapter 5

Discussion

In this chapter, the results obtained in Chapter 4 are compared to studies performed by other authors and with experimental data. The findings in this study are also discussed.

5.1 Parameter fit compared with literature values

The bulk modulus and its pressure derivatives found from the least square evaluation (see Table 4.1.1) have also been obtained by others, e.g. Holland & Powell (2011). The parameter values found from their evaluation are shown in Table 5.1.1.

Table 5.1.1: Values obtained by Holland & Powell (2011) and from this study

	Holland & Powell			This study		
Substance	K_0	K_0'	K_0''	K_0	K_0'	K_0''
MgO	161.6	3.95	−0.024	160	3.9	−0.003
CaO	113	3.87	−0.034	109.4	4.9	−0.028
Al_2O_3(corundum)	254	4.34	−0.017	270	4.4	−0.013
SiO_2(α-quartz)	73	6.00	−0.082	39	6.0	−0.2
NaCl	23.8	5.00	−0.21	24.4	5.0	−0.05
$MgCO_3$	102.8	5.41	−0.053	112	4.8	−0.02

By comparing Table 4.1.1 and Table 5.1.1 it can be seen that for the parameter K_0 the solids Al_2O_3, SiO_2 and $MgCO_3$ lies outside the uncertainty boundaries in Table 4.1.1. Al_2O_3 and $MgCO_3$ do not lie far from the uncertainty boundaries, but they are still not within. The most interesting deviation for the bulk modulus is still for SiO_2. The value of K_0 in the current evaluation is just one half from the one obtained by Holland & Powell (2011). This value has therefore been compared to other studies which confirm the findings here. The bulk modulus for SiO_2 was found by other authors to be 37.2 GPa (Liu 1993) , 39.7 GPa (Newton, O'Keeffe & Gibbs 1980) and 36.2 GPa (Meng, Bernazzani, a O'Connell, McKenna & Simon 2009). Based on this it seem to be a misprint in Holland & Powell (2011) for that particular solid.

For the K_0' all the values except for CaO lie within the standard deviation for the parameters found by regression. The values for CaO are very close to the uncertainty boundary, but not within. No evidence is found in this study as to why this value should not conform to our fit.

By comparing the K_0'' values found through this study with Holland & Powell's study larger deviations can be found. This can be explained by the fact that in Holland & Powell (2011), a heuristic model for the K_0'' value was used. The heuristic model was $K_0'' = -\frac{K_0}{K_0'}$. Thus, a direct comparison between the values obtained here, and the ones found in their paper will give large deviations. This is due to the fact that Holland & Powell's study is only a regression on two parameters, i.e. K_0 and K_0', while this study does regression on all three parameters directly. Independent of this difference there exists a fundamental criterion that must be satisfied for all substances, $\left(\frac{\partial^2 K}{\partial p^2}\right) < 0$ (Stacey 2004). In the parameter fitting procedure presented here, this criterion has been fulfilled for all solids investigated (see Table 4.1.1).

5.2 Isothermal EOSs and uncertainty vectors

As seen from Figures 4.2.1 through 4.2.6 it is difficult to determine which two-parameter EOS gives the best fit when the uncertainty in the parameters are taken into consideration. The Birch-Murnaghan, Vinet and pseudo-spinodal EOS all seem to give reasonable results depending on the solid considered. A general conclusion about which EOS gives the best fit for all substances based only on the deviation plots can therefore not be drawn. Other elements were therefore needed to be taken into considerations before choosing a two-

parameter complete EOS to use for later predictions of substances at high pressure and high temperature. The pseudo-spinodal has an advantage over the Birch–Murnaghan and Vinet EOS because of its ability to be inverted (see Section 2.2). It also feature a promising way of including thermal effects.

The shaded area of the plots given in Figures 4.2.1 through 4.2.6 are as described in Section 4.2 made from three decorrelated eigenvectors of the covariance matrix. In this context, decorrelation means that the variables has been scaled and rotated such that they no longer depend on each other. The same decorrelation has been used for both the bootstrap and the maximum likelihood method. It is based on the eigenvectors and eigenvalues of the covariance matrix. The parameter uncertainties ($\Delta\underline{\theta_i}$) are calculated as follows:

$$\Delta\underline{\theta_i} = Q(\sqrt{\Lambda})^{-1} e_i \tag{5.2.1}$$

Here, Q is the eigenvector matrix and Λ are the eigenvalues of the covariance matrix. The e_i is the i'th unit vector. The same contour lines as shown in Figure 4.1.1 have been replotted with comparative axes in Figure 5.2.1.

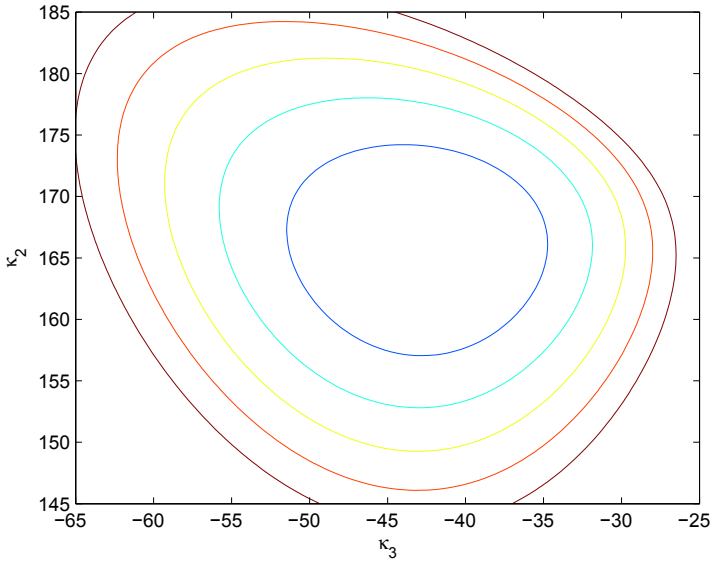

Figure 5.2.1: Contour plot for κ_2 versus κ_3 with κ_1 constant for MgO in the scaled and rotated coordinates

From Figure 5.2.1 it can be seen that the contours are more like concentric circles

compared to Figure 4.1.1. The deviation from the circular shape away from optimum is due to nonlinearity of the objective function given in Equation 4.1.2. For a quadratic function the contours would have been truly concentric over the scale.

The maximum difference in the uncertainty vectors calculated from the bootstrap and the maximum likelihood method was found to be $\pm 5 - 65\%$ for all the solids investigated except for MgO. For MgO the ratio between the methods was at the most a factor of 2.1. This can be explained by the rejection of the null hypothesis as shown in Section 5.4. The fact that the results are similar for two statistical methods gives no guarantee that the calculation of the variance is correct, but it gives an indication that the statistics have been used correctly.

5.3 The complete EOS and comparison with experimental data

To test the predictions made for the thermodynamic functions in Section 4.3 some of them are compared to experimental data. Experimental data for the thermal expansion as a function of temperature at ambient pressure was found for NaCl (Anderson 1995) and MgO (Anderson & Zou 1989). These data were plotted against the ambient pressure predictions made from the pseudo-spinodal and the first order Murnaghan EOS expanded with an Einstein temperature dependency.

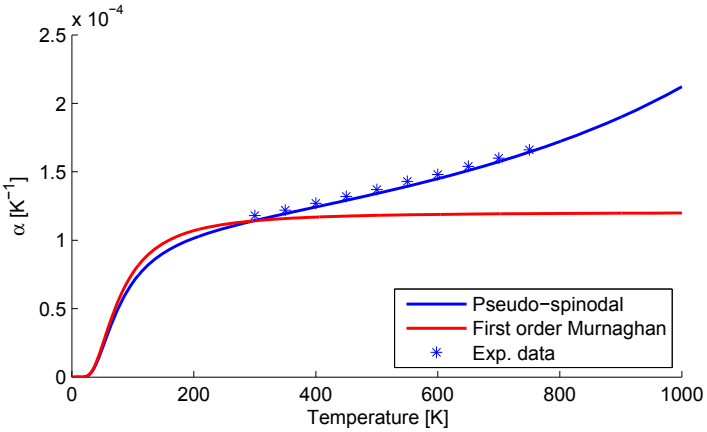

Figure 5.3.1: Thermal expansion, α, as a function of temperature for NaCl at ambient pressure

From Figure 5.3.1 it can be seen that for NaCl the prediction of thermal expansion from the pseudo-spinodal EOS provides a good fit to the experimental data. The first order Murnaghan equation has been plotted for comparison. At low temperatures the two EOS has the same behaviour due to the same Einstein function, but at higher temperatures the pseudo-spinodal follows the experimental data much better. The reason for the better fit comes from the incorporation of thermal effects into the pseudo-spinodal pressure(p_{sp}).

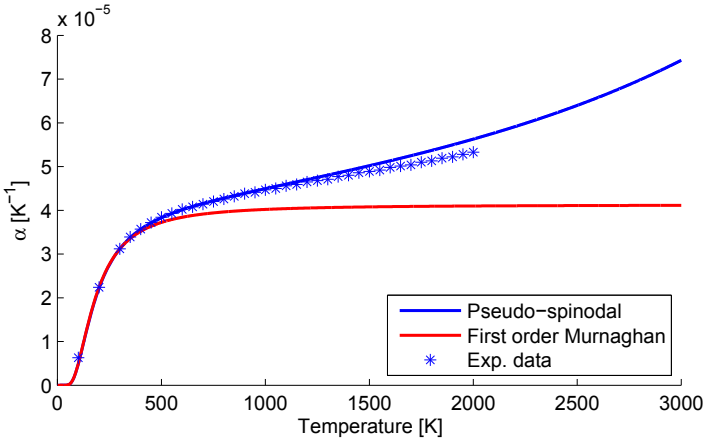

Figure 5.3.2: Thermal expansion, α, as a function of temperature for MgO at ambient pressure

From Figure 5.3.2 it can be seen that for MgO the prediction of thermal expansion from the pseudo-spinodal EOS gives an accurate fit to the experimental data up to approximately 1500 K. Beyond this temperature the pseudo-spinodal EOS overestimate the thermal expansion for MgO. This can be explained by the fact that $\frac{\gamma^0}{V_0}$ is assumed constant in the pseudo-spinodal EOS whilst it actually varies slightly with temperature.

The reason why the thermal expansion for NaCl fits better to the experimental data than for MgO can be explained from the temperature behaviour of the Grüneisen parameter (γ). For alkali halides, e.g. NaCl, the Grüneisen parameter generally decreases with temperature. For oxides on the other hand, e.g. MgO, the Grüneisen parameter increases with temperature (Anderson 1995). This opposite temperature effect on the Grüneisen parameter for oxides and alkali halides has implications on the model predictions within the framework of the pseudo-spinodal EOS and how good they fit to experimental data. This can be seen by comparing Figure 5.3.1 and Figure 5.3.2. From the results obtained here it is natural to assume that the pseudo-spinodal EOS gives better predictions for alkali

halides than for oxides. To test this assumption completely it is recommended in further work to test for other alkali halides and oxides.

For NaCl, experimental data as a function of pressure at ambient temperature were also found in the literature (Boehler & Kennedy 1980). These data have been plotted against the predictions from the pseudo-spinodal EOS, and are shown in Figure 5.3.3.

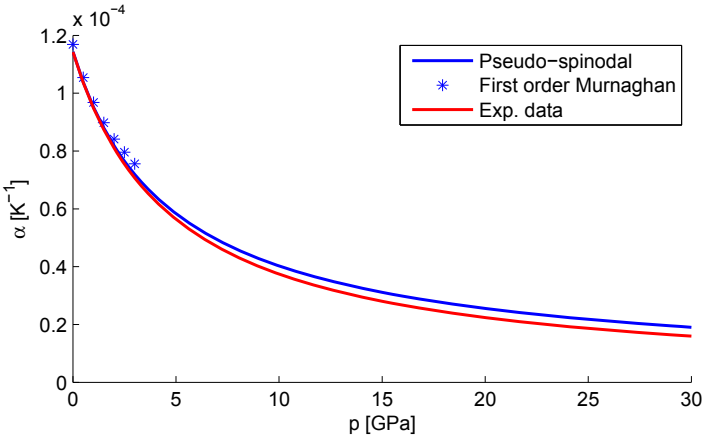

Figure 5.3.3: Thermal expansion, α, as a function of pressure for NaCl

From Figure 5.3.3 it can be seen that both the first order Murnaghan and the pseudo-spinodal EOS give accurate fit to the data. This is due to the low pressure that the thermal expansion has been measured at. However, it may seem like the experimental data follow the curve from the pseudo-spinodal better if they are extrapolated to higher pressures.

Measurements of compression at both high pressure and high temperature were found for NaCl (Boehler & Kennedy 1980) and MgO (Fei 1999). For NaCl pressure-volume data was found at several different temperatures, whilst for MgO it was found at 298 and 1100 K. This data has been plotted together with the pressure-volume-temperature predictions from the pseudo-spinodal EOS in Figures 5.3.4 and 5.3.5 respectively.

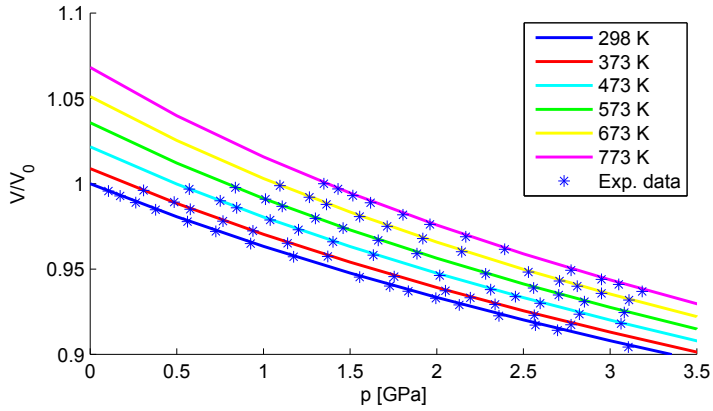

Figure 5.3.4: Compression as a function of pressure at different temperatures for NaCl

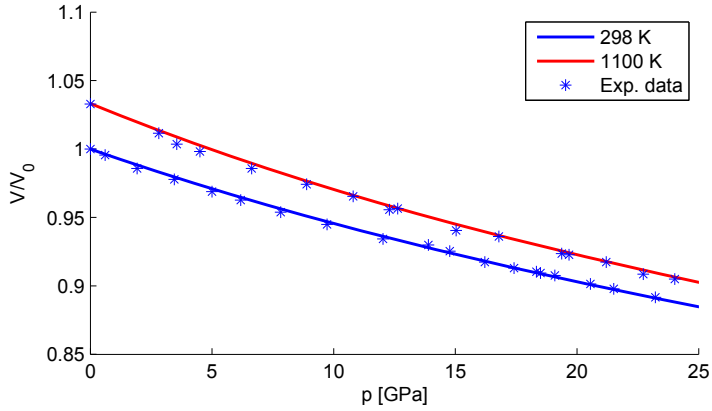

Figure 5.3.5: Compression as a function of pressure at two different temperatures for MgO

From Figures 5.3.4 and 5.3.5 it is evident that the predictions are in excellent agreement with the experimental data. This confirms that the pseudo-spinodal EOS can predict the pressure-volume-temperature surface reliably for the solids in question. The only issue is that the pressures for which experimental data are available at high temperatures are quite low. Thus, it does not give a significant difference between which of the isothermal EOSs in this study that is used as long as the same temperature dependency is introduced (see Figures 4.2.1 and 4.2.5).

From the aforementioned discussion of the predicted thermodynamic functions and their conformation to experimental data it may seem that the pseudo-spinodal EOS is a good

foundation for a general EOS. However, it turns out to be an inconsistency in the implementation of the Einstein model as a description of the internal energy. At very high pressures the heat capacity becomes negative at low temperatures. This effect is difficult to discover at the pressure range used in Figures 4.3.4a and 4.3.1a. By comparing the isobaric heat capacity at ambient pressure and at 1000 GPa the inconsistency becomes evident. In Figure 5.3.6 the isobaric heat capacity has been plotted at ambient and 1000 GPa.

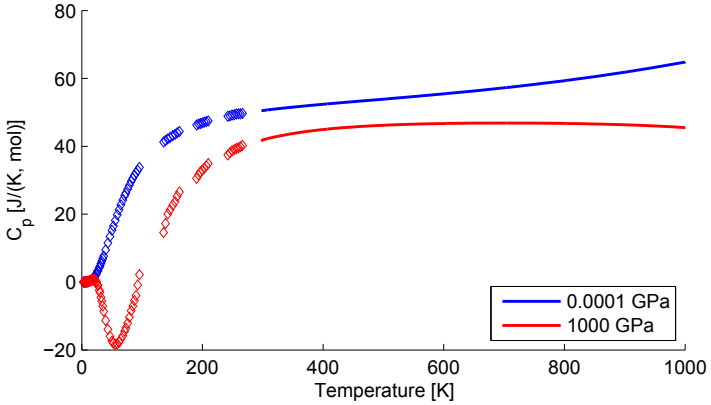

Figure 5.3.6: Heat capacity, C_p, as a function of temperature at ambient pressure for NaCl

By testing the prediction of heat capacity at high pressure for MgO as well as NaCl it can be seen the same effect at low temperatures as can be seen in Figure 5.3.7.

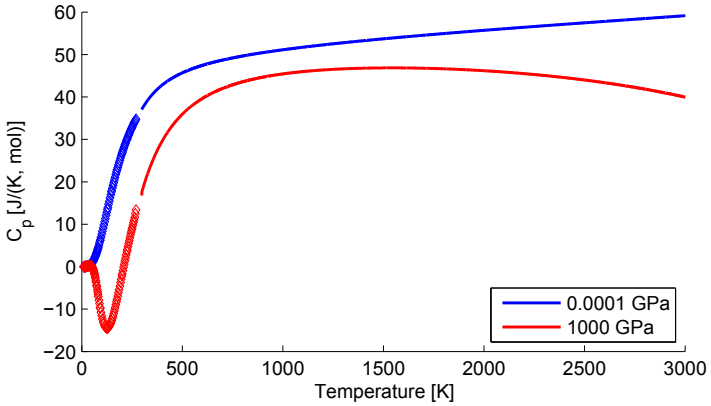

Figure 5.3.7: Heat capacity, C_p, as a function of temperature at ambient pressure for MgO

This inconsistency in the pseudo-spinodal EOS has not been discussed in any previous

papers known to the author. The problem discovered here imposes serious limitations on the use of the pseudo-spinodal EOS. Even though the effect of negative isobaric heat capacity only appears at high pressures, it still violates one of the thermodynamic stability criterion. The two stability criterion which must be fulfilled for a stable thermodynamic system given in Helmholtz potential are as follows (Callen 1985):

$$\left(\frac{\partial^2 A}{\partial T^2}\right)_V \leq 0 \quad \left(\frac{\partial^2 A}{\partial V^2}\right)_T \geq 0 \tag{5.3.1}$$

By rewriting the stability criterion in Equation 5.3.1 into the thermodynamic quantities it can be seen that:

$$C_p \geq 0 \quad K \geq 0 \tag{5.3.2}$$

Thus, both the isobaric heat capacity and the isothermal bulk modulus must be positive for a stable system. From Figures 4.3.3a and 4.3.3b it can be seen that the bulk modulus is always positive in the range of pressures tested for MgO, but the heat capacity becomes negative in a certain range of temperatures at high pressure. Thus, the thermodynamic stability criterion from Equation 5.3.2 is violated. The discussion on thermodynamic stability is a field of its own and lies outside the scope of this thesis, but is still important for further evaluation.

The inconsistency in the EOS can also be shown through an evaluation of the total differential for entropy as given in Equation 5.3.3.

$$-\mathrm{d}S = \left(\frac{\partial^2 A}{\partial T^2}\right)_V \mathrm{d}T + \left(\frac{\partial^2 A}{\partial T \partial V}\right)_T \mathrm{d}V \tag{5.3.3}$$

If the differential in Equation 5.3.3 is a total differential the following relation must be true:

$$\left(\frac{\partial^3 A}{\partial T \partial T \partial V}\right)_T = \left(\frac{\partial^3 A}{\partial T \partial V \partial T}\right)_V \tag{5.3.4}$$

When the Einstein model is used to predict the heat capacity the heat capacity is only a function of temperature, whilst the calculated heat capacity is a function of both temperature and pressure. The left hand side of Equation 5.3.4 can be calculated as follows:

$$\left(\frac{\partial^3 A}{\partial T \partial T \partial V}\right)_T = \left(\frac{\partial \frac{-C_V(T,V)}{T}}{\partial V}\right)_T = g(T,V) \tag{5.3.5}$$

The right hand side of Equation 5.3.4 can be written as follows:

$$\left(\frac{\partial^3 A}{\partial T \partial V \partial T}\right)_V = \left(\frac{\partial -\left(\frac{\partial p}{\partial T}\right)_V}{\partial T}\right)_V = f(T) \tag{5.3.6}$$

By comparing Equation 5.3.5 and Equation 5.3.6 it can be seen that there exists an inconsistency since the latter equation is only a function of T, whilst the first is a function of both T and V. Thus, an inconsistency in the EOS is present.

In further work it is recommended to search for a consistent way to include the internal energy or the heat capacity in the pseudo-spinodal EOS. Together with the high accuracy of predictions for the pseudo-spinodal EOS, a consistent model will be a valuable asset in the prediction of high pressure and high temperature effects on solids.

5.4 Chi-square goodness of fit test

The pressure-volume data that are used for the testing of the isothermal EOSs have been assumed to have a normal distribution. This assumption was used to find the standard deviations for the parameters given in Table 4.1.1. To test if the population actually is normally distributed a χ^2 goodness of fit test can be utilized. This method is based how good a fit there is between the frequency of observations in the observed sample and the expected frequencies obtained from the hypothesized distribution (Walpole et al. 2007). In this case, the hypothesized distribution is the normal distribution. The quantity tested is the χ^2 value given in Equation 5.4.1.

$$\chi^2 = \sum_{i=1}^{k} \frac{(O_i - E_i)^2}{E_i} \tag{5.4.1}$$

The χ^2 is a random variable whose sampling distribution is very close to the chi-squared distribution with $k - 1$ degrees of freedom. O_i and E_i are the observed and expected frequencies for bin number i.

The null hypothesis used in our test case is that the observed samples come from a normal distribution. With a 0.05 significance level the critical region for rejecting the null hypothesis, H_0, is $\chi^2 > \chi^2_{0.05}$. This decision criterion require that each of the expected frequencies are at least 5 or above to be valid (Walpole et al. 2007). If the expected frequencies are lower than 5 the adjacent bins should be merged, and as a result the degrees of freedom reduces accordingly. Thus, the degrees of freedom become "number of bins" minus one. The pressure-volume datasets for the different substances were all tested in this manner and the results of the hypothesis tests are shown in Table 5.4.1.

Table 5.4.1: χ^2 test for normal distribution

Substance	χ^2 (calculated)	degrees of freedom	$\chi^2_{0.05}$	H_0
MgO	76.6688	8	15.507	Rejected
CaO	1.3713	3	7.815	Not rejected
Al_2O_3	2.6255	5	11.070	Not rejected
SiO_2	1.9394	3	7.815	Not rejected
NaCl	5.4016	5	11.070	Not rejected
$MgCO_3$	9.5658	5	11.070	Not rejected

From Table 5.4.1 it can be seen that for all solids except MgO the hypothesis of normal distribution cannot be rejected. This affects the maximum likelihood method since this method assumes normally distributed data. The bootstrap has the advantage over the maximum likelihood method that it is distribution independent. Thus, the uncertainty vectors in Table 4.1.1 were calculated using the bootstrap method. The normal cumulative distribution function has been plotted together with the standarized experimental data for CaO and MgO in Figures 5.4.1a and 5.4.1b respectively. These two has been shown since they give the best and worse fit to the normal distribution, as can be seen in Table 5.4.1.

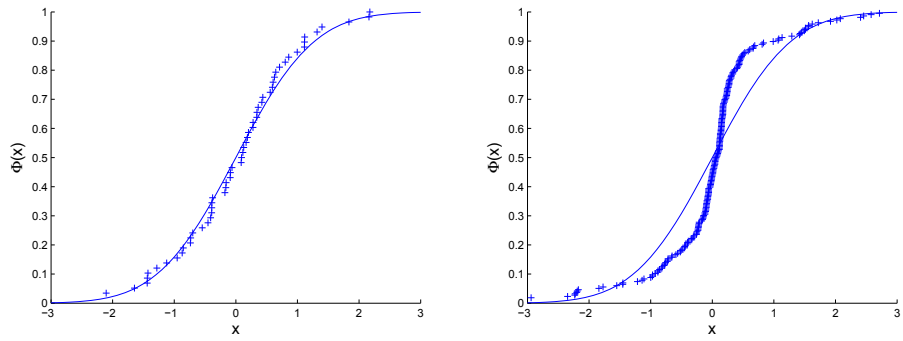

(a) CaO (b) MgO

Figure 5.4.1: The normal cumulative distribution function plotted together with the standarized experimental data

Chapter 6

Conclusion

In this thesis, different two-parameter EOSs were tested for different solids. A second order Murnaghan EOS was used for parameter fitting. The standard deviation of the parameters was found based on diagonalization of the covariance matrix found from either the maximum likelihood or the bootstrap method. These two methods gave comparable results for the standard deviation for the parameters($\pm 5-65\%$) except for MgO which was found to reject the null hypothesis of normal distribution. Since the maximum likelihood method is based on an assumption of normal distribution, whilst the bootstrap method is not, the results obtained from the bootstrap were reported.

This evaluation showed that none of the isothermal EOSs were found to provide better fit, compared to the other EOSs, for all the solids when uncertainty in the parameters was taken into account. Regardless of this fact, the isothermal pseudo-spinodal EOS was chosen as the basis for a complete EOS. This was done due to the pseudo-spinodal EOS ability to be inverted and to predict high temperature properties with only room temperature data as input.

The heat capacity, thermal expansion and the isothermal bulk modulus were predicted at high pressure and temperature for NaCl and MgO. The thermal expansion and the complete pressure-volume-temperature surface predicted were also compared with available experimental data. The predictions gave good fit to the data. From this analysis it may seem that the pseudo-spinodal EOS gives better fit for alkali halides than for oxides due to the difference in thermal dependency of the Grüneisen parameter for these two substance groups.

The major finding in this report was that an inconsistency in the pseudo-spinodal EOS was found at high pressure. The EOS predicted negative heat capacity at very high pressures and low temperature. It is recommended in further work to search for a consistent way of including internal energy. This will provide an EOS of great value in the prediction of high pressure and high temperature effects on solids.

Bibliography

Anderson, O. L. (1995), *Equations of state of solids for geophysics and ceramic science*, Oxford university press.

Anderson, O. L. & Zou, K. (1989), 'Formulation of the thermodynamic functions for mantle minerals: Mgo as an example', *Physical chemistry of minerals* **16**, 642–648.

Baonza, V. G. (2012), 'Discussion on the rupture pressure', [Letter]. (Personal communication, 7. May 2012).

Baonza, V. G., Alonso, M. C. & Nunez, J. (1994), 'Universal behaviour of compressed liquids', *The journal of physical chemistry* **98**, 4955–4958.

Baonza, V. G., Taravillo, M., Caceres, M. & Nunez, J. (1995), 'Universal features of the equation of state of solids from a pseudospinodal hypothesis', *Physical review B* **53**, 5252–5257.

Barron, T. H. K., Berg, W. T. & Morrison, J. A. (1959), 'On the heat capacity of crystalline magnesium oxide', *Proceedings of the royal society of london. Series A, Mathematical and physical sciences* **250**, 70–83.

Barron, T. H. K., Leadbetter, A. J. & Morrison, J. A. (1964), 'The thermal properties of alkali halide crystals', *Proceedings of the royal society of London* **279**, 62–81.

Birch, F. (1947), 'Finite elastic strain of cubic crystals', *Physical review* **71**, 809–824.

Birch, F. (1986), 'Equation of state and thermodynamic parameters of NaCl to 300 kbar in the high-temperature domain', *Journal of geophysical research* **91**, 4949–4954.

Boehler, R. & Kennedy, G. C. (1980), 'Equation of state of sodium chloride up to 32 kbar and 500 ^{0}c', *Journal of physical chemistry of solids* **41**, 517–523.

Callen, H. B. (1985), *Thermodynamics and an introduction to thermostatistics*, John Wiley & Sons.

Chase, M. W. (1998), 'Nist-janaf thermochemical tables', *Journal of physical and chemical reference data* **9**, 1–1951.

Chauhan, R. S., Lal, K. & Singh, C. P. (2011), 'Inverted equations of state for solids under high pressure', *Indian journal of physics* **85**, 1341–1366.

d'amour, H., Schiferl, D., Denner, W., Schulz, H. & Holzapfel, W. B. (1978), 'High pressure single crystal structure determinations for ruby up to 90 kbar using an automatic diffractometer', *Journal of applied physics* **49**, 4411–4415.

Efron, B. & Tibshirani, R. J. (1993), *An introduction to the bootstrap*, Chapman & Hall/CRC.

Fei, Y. (1999), 'Effects of temperature and composition on the bulk modulus of (mg,fe)o', *American mineralogist* **84**, 272–276.

Fiquet, G. & Reynard, B. (1999), 'High-pressure equation of state of magnesite: new data and a reappraisal', *American mineralogist* **84**, 856–860.

Fuchizaki, K. (2006), 'Murnaghan's equation of state revisted', *Journal of the physical society of Japan* **75**, –.

Golder, M. (n.d.), 'Maximum likelihood estimation (mle)', [pdf] Available at: `https://files.nyu.edu/mrg217/public/mle_introduction1.pdf` [Accessed 10 May 2012].

Grevel, K. D., Burchard, M., Fasshauer, D. W. & Peun, T. (2000), 'Pressure-volume-temperature behaviour of diaspore and corundum: an in situ x-ray diffraction study comparing different pressure media', *Journal of geophysical research* **105**, 27877–27887.

Hart, H. V. & Drickamer, H. G. (1965), 'Effect of high pressure on the lattice parameters of al2o3', *Journal of chemical physics* **43**, 2265–2266.

Haug-Warberg, T. (2006), *Den termodynamiske arbeidsboken*, Kolofon forlag AS.

Hazen, R. M., Finger, L. W., Hemley, R. J. & Mao, H. K. (1989), 'High-pressure crystal chemistry and amorphization of α quartz', *Solid state communication* **72**, 507–511.

Hofmeister, A. M. (1993), 'Interatomic potentials calculated from equations of state: limitation of finite strain to moderate k", *Geophysical research letter* **20**, 635–638.

Holland, T. J. B. & Powell, R. (2011), 'An improved and extended internally consistent thermodynamic dataset for phases of petrological interest, involving a newequation of state for solids', *Journal of metamorphic geology* **29**, 333–383.

Jacobsen, S. D., Holl, C. M., Adams, K. A., Fischer, R. A., Martin, E. S., Bina, C. R., Lin, J.-F., Prakapenka, V. B., Kubo, A. & Dera, P. (2008), 'Compression of single-crystal magnesium oxide to 118 gpa and a ruby pressure gauge for helium pressure media', *American mineralogist* **93**, 1823–1828.

Kushwah, S. S. & Sharma, M. P. (2012), 'Volume dependence of the grüneisen parameter for mgo', *Solid state communications* **152**, 414–416.

Levien, L., Prewitt, C. T. & Weidner, D. J. (1980), 'Structure and elastic properties of quartz at pressure', *American mineralogist* **65**, 920–930.

Li, B., Wood, K. & Kung, J. (2006), 'Elasticity of mgo to11 gpa with an independent absoulute pressure scale: Implications for pressure calibration', *Journal of geophysical research* **111**, B11206.

Liu, L. (1993), 'Bulk moduli of sio_2 polymorphs: quartz, coesite and stihovite', *Mechanics of materials* **14**, 283–290.

Liu, L. & Basset, W. A. (1973), 'Compression of ag and phase transformation of nacl', *Journal of applied physics* **44**, 1475–1479.

Mammone, J. F., Mao, H. K. & Bell, P. M. (1981), 'Equations of state of cao under static pressure conditions', *Geophysical research letter* **8**, 140–142.

Mao, H. K. & Bell, P. M. (1979), 'Equations of state of mgo and ϵ fe under static pressure conditions', *Journal of geophysical research* **84**, 4533–4536.

Marsh, S. P. (1980), *Lasl shoch hugoniot data*, University of california press.

Meng, Y., Bernazzani, P., a O'Connell, P., McKenna, G. B. & Simon, S. L. (2009), 'A new pressurizable dilatometer for measuring the time-dependent bulk modulus and pressure-volume-temperature properties of polymeric materials', *Review of scientific instruments* **80**, 053903.

Mills, I., Cvitas, T., Homann, K., Kallay, N. & Kuchitsu, K. (1993), *Quantities, Units and Symbols in Physical Chemistry*, Blackwell science Ltd.

Murnaghan, F. D. (1944), 'The compressibility of media under extreme pressure', *Proceedings of the national academy of science* **30**, 244–247.

Newton, M. D., O'Keeffe, M. & Gibbs, G. V. (1980), 'Ab initio calculations of interatomic force constants in $h_6si_2o_7$ and the bulk modulus of α-quartz and α-cristobalite', *Physical chemistry of minerals* **6**, 305–312.

Olinger, B. & Halleck, P. M. (1976), 'The compression of α quartz', *Journal of geophysical research* **81**, 5711–5714.

Perezalbuerne, E. A. & Drickamer, H. G. (1965), 'Effect of high pressures on the compressibilities of seven crystals having the nacl or cscl structure', *The journal of chemical physics* **43**, 1381–1387.

Plymate, T. G. & Stout, J. H. (1989), 'A five-parameter temperature-corrected murnaghan equation for p-v-t surfaces', *Journal of geophysical research* **94**, 9477–9483.

Richet, P., Mao, H.-K. & Bell, P. M. (1988), 'Static compression and equation of state of cao to 1.35 mbar', *Journal of geophysical research* **93**, 15279–15288.

Richet, P., Xu, J. A. & Mao, H.-K. (1988), 'Quai-hydrostatic compression of ruby to 500 kbar', *Physics and chemistry of minerals* **16**, 207–211.

Ross, N. L. (1997), 'The equation of state and high-pressure behaviour of magnesite', *American mineralogist* **82**, 682–688.

Rottmann, K. (2006), *Matematisk formelsamling*, Spektrum forlag.

Sato-Sorensen, Y. (1983), 'Phase transition and equation of state for the sodium halides: Naf, nacl, nabr, and nai', *Journal of geophysical research* **88**, 3543–3548.

Sato, Y. & Akimoto, S. (1979), 'Hydrostatic compression of four corundumtype compounds: αal2o3, v2o3, cr2o3, and αfe2o3', *Journal of applied physics* **50**, 5285–5291.

Speedy, R. J. (1982), 'Limiting forms of the thermodynamic divergences at the conjectured stability limits in superheated and supercooled water', *Journal of physical chemistry* **86**, 3002–3005.

Speziale, S., Shieh, S. R. & Duffy, T. S. (2006), 'High-pressure elasticity of calcium oxide: A comparison between brillouin sopectroscopy and radial x-ray diffraction', *Journal of geophysical research* **111**, B02203.

Speziale, S., Zha, C.-S., Duffy, T. S., Hemley, R. J. & Mao, H.-K. (2001), 'Quasi-hydrostatic compressionof magnesium oxide to 52 gpa: Implications for the pressure-volume-temperature equation of state', *Journal of geophysical research* **106**, 512–528.

Stacey, F. D. (2004), 'High pressure equations of state and planetary interiors', *Reports on progress in physics* **68**, 341–383.

Taravillo, M., Baonza, V. G., Rubio, J. E. F., Nunez, J. & Caceres, M. (2001), 'The temperature dependence of the equation of state at high pressures revisted: a universal model for solids', *Journal of physics and chemistry of solids* **63**, 1705–1715.

Vinet, P. & Ferrante, J. (1987), 'Compressibility of solids', *Journal of geophysical research* **92**, 9319–9325.

Vinet, P., Smith, J. R., Ferrante, J. & Rose, J. H. (1986), 'Temperature effects on the universal equation of state of solids', *PhysRevBCondensMatter* **35**, 1945–1953.

Wackerle, J. (1962), 'Shochwave compression of quartz', *Journal of applied physics* **33**, 922–937.

Walpole, R. E., Myers, R. H., Myers, S. L. & Ye, K. (2007), *Probability & statistics for engineers & scientists*, Pearson education international.

Wedepohl, P. T. (1976), 'Accuracy of the murnaghan equation compared with that of an exponential equation of state', *Journal of Physics D: Applied physics* **10**, 43–48.

Yamanaka, T., Kittaka, K. & Nagai, T. (2002), 'B1-b2 transition in cao and possibility of $casio_3$-perovskite decomposition under high pressure', *Journal of mineralogical and petrological sciences* **97**, 144–152.

Appendix A

Pressure-volume data for the isothermal curve fitting

In this appendix the experimental pressure-volume data that is used for the isothermal curve fitting is given in the following tables. The tables show the data and the references from were the data is found.

Table A.1: Experimental pressure-volume data for MgO at T = 300 K

no.	**Pressure**	$(\frac{V}{V_0})$	**Ref**	**no.**	**Pressure**	$(\frac{V}{V_0})$	**Ref**
1	0.8	0.9964	1	2	1.3	0.9909	1
3	3.1	0.9807	1	4	4.5	0.9724	1
5	5.7	0.9659	1	6	6.6	0.9601	1
7	7.6	0.9548	1	8	8.3	0.9524	1
9	9.5	0.9467	1	10	10.0	0.9463	1
11	5.7	0.9662	1	12	8.7	0.9532	1
13	10.6	0.9431	1	14	12.5	0.9349	1
15	16.0	0.9198	1	16	18.1	0.9093	1
17	20.1	0.9032	1	18	21.9	0.8973	1
19	24.0	0.8887	1	20	26.4	0.8814	1

Continued on next page

Table A.1 – *Continued from previous page*

no.	Pressure	$(\frac{V}{V_0})$	Ref	no.	Pressure	$(\frac{V}{V_0})$	Ref
21	29.1	0.8718	1	22	31.2	0.865	1
23	33.2	0.8593	1	24	35.2	0.8537	1
25	37.1	0.848	1	26	39.4	0.8417	1
27	41.7	0.8351	1	28	43.3	0.8297	1
29	46.8	0.8212	1	30	48.3	0.8172	1
31	50.4	0.8115	1	32	52.2	0.8071	1
33	43.7	0.836	2	34	53.8	0.814	2
35	56.1	0.812	2	36	73.4	0.78	2
37	74.5	0.779	2	38	82.9	0.764	2
39	86.3	0.77	2	40	94.1	0.748	2
41	2.5	0.987	3	42	5.0	0.974	3
43	7.5	0.963	3	44	10.0	0.951	3
45	15.0	0.93	3	46	20.0	0.91	3
47	25.0	0.893	3	48	30.0	0.877	3
49	35.0	0.862	3	50	1.7	0.99	4
51	3.78	0.978	4	52	5.17	0.97	4
53	6.23	0.962	4	54	8.29	0.954	4
55	8.89	0.952	4	56	10.95	0.942	4
57	8.96	0.951	4	58	8.42	0.954	4
59	7.47	0.959	4	60	6.54	0.963	4
61	5.63	0.968	4	62	5.73	0.968	4
63	3.86	0.978	4	64	5.24	0.97	4
65	3.05	0.982	4	66	2.29	0.987	4
67	8.5	0.953	4	68	12.4	0.9346	4
69	15.7	0.9205	4	70	18.5	0.9091	4

Continued on next page

Table A.1 – *Continued from previous page*

no.	Pressure	$(\frac{V}{V_0})$	Ref	no.	Pressure	$(\frac{V}{V_0})$	Ref
71	23.6	0.89	4	72	28.3	0.8739	4
73	30.3	0.8677	4	74	35.5	0.8518	4
75	39.1	0.8418	4	76	42.0	0.8339	4
77	44.8	0.8266	4	78	48.7	0.817	4
79	52.1	0.8089	4	80	55.1	0.8023	4
81	58.1	0.7956	4	82	61.7	0.7881	4
83	65.3	0.7809	4	84	68.2	0.7754	4
85	71.3	0.7695	4	86	6.6	0.9625	4
87	8.6	0.9528	4	88	11.7	0.938	4
89	13.5	0.93	4	90	18.9	0.9076	4
91	23.0	0.8923	4	92	27.8	0.8756	4
93	4.4	0.9744	4	94	8.4	0.9536	4
95	12.1	0.9359	4	96	18.3	0.91	4
97	24.4	0.8872	4	98	31.5	0.8639	4
99	37.6	0.8458	4	100	41.4	0.8355	4
101	45.9	0.824	4	102	48.7	0.817	4
103	53.2	0.8066	4	104	57.1	0.7978	4
105	60.3	0.791	4	106	65.3	0.781	4
107	69.4	0.773	4	108	72.8	0.7667	4
109	78.9	0.756	4	110	84.0	0.7475	4
111	90.1	0.7378	4	112	94.4	0.7313	4
113	102.9	0.7191	4	114	106.4	0.7144	4
115	109.4	0.7104	4	116	113.8	0.7047	4
117	118.1	0.6993	4	118	8.5	0.953	4
119	12.2	0.9346	4	120	15.3	0.9205	4

Continued on next page

Table A.1 – *Continued from previous page*

no.	Pressure	$(\frac{V}{V_0})$	Ref	no.	Pressure	$(\frac{V}{V_0})$	Ref
121	18.2	0.9091	4	122	23.4	0.89	4
123	28.1	0.8739	4	124	29.9	0.8677	4
125	34.5	0.8518	4	126	37.6	0.8418	4
127	40.4	0.8339	4	128	42.9	0.8266	4
129	46.9	0.817	4	130	49.7	0.8089	4
131	53.0	0.8023	4	132	56.1	0.7956	4
133	59.5	0.7881	4	134	62.8	0.7809	4
135	65.6	0.7754	4	136	68.3	0.7695	4
137	6.5	0.9625	4	138	8.4	0.9528	4
139	11.5	0.938	4	140	13.3	0.93	4
141	18.6	0.9076	4	142	22.6	0.8923	4
143	27.4	0.8756	4	144	4.3	0.9744	4
145	7.9	0.9536	4	146	11.6	0.9359	4
147	17.8	0.91	4	148	23.9	0.8872	4
149	30.6	0.8639	4	150	36.5	0.8458	4
151	40.1	0.8355	4	152	43.7	0.824	4
153	46.8	0.817	4	154	51.0	0.8066	4
155	55.3	0.7978	4	156	58.4	0.791	4
157	62.9	0.781	4	158	66.5	0.773	4
159	69.6	0.7667	4	160	74.6	0.756	4
161	80.0	0.7475	4	162	85.0	0.7378	4
163	89.0	0.7313	4	164	96.2	0.7191	4
165	99.6	0.7144	4	166	102.4	0.7104	4
167	106.3	0.7047	4	168	111.0	0.6993	4
169	3.6	0.9786	5	170	7.4	0.9611	5

Continued on next page

Table A.1 – *Continued from previous page*

no.	Pressure	$(\frac{V}{V_0})$	Ref	no.	Pressure	$(\frac{V}{V_0})$	Ref
171	10.6	0.9452	5	172	13.5	0.932	5
173	16.2	0.9196	5	174	18.9	0.9084	5
175	22.8	0.8949	5	176	26.9	0.8807	5
177	31.1	0.8666	5	178	36.6	0.8507	5
179	41.4	0.8377	5	180	49.1	0.8201	5
181	52.2	0.8127	5	182	53.5	0.8098	5
183	55.9	0.8041	5	184	58.1	0.7981	5
185	61.1	0.7933	5	186	63.5	0.7876	5
187	65.9	0.783	5	188	68.7	0.7798	5
189	71.2	0.7729	5	190	73.9	0.7676	5
191	76.2	0.7646	5	192	80.1	0.7578	5
193	83.5	0.7511	5	194	86.6	0.7469	5
195	18.87	0.9068	6	196	19.76	0.8997	6
197	20.06	0.9007	6	198	20.04	0.8997	6
199	26.92	0.8764	6	200	28.83	0.8733	6
201	31.05	0.8642	6	202	46.26	0.8319	6
203	44.71	0.8227	6	204	49.88	0.8238	6
205	50.64	0.8187	6	206	59.15	0.7985	6
207	65.7	0.7863	6	208	75.12	0.7722	6
209	82.54	0.757	6	210	85.3	0.7581	6
211	87.27	0.753	6	212	88.16	0.75	6
213	91.71	0.7439	6	214	94.66	0.7429	6
215	106.6	0.7237	6	216	110.1	0.7197	6
217	120.4	0.7066	6	218	121.8	0.7055	6

[1] (Speziale, Zha, Duffy, Hemley & Mao 2001)
[2] (Mao & Bell 1979)
[3] (Perezalbuerne & Drickamer 1965)
[4] (Li, Wood & Kung 2006)
[5] (Jacobsen, Holl, Adams, Fischer, Martin, Bina, Lin, Prakapenka, Kubo & Dera 2008)
[6] (Marsh 1980)

Table A.2: Experimental pressure-volume data for CaO at T = 300 K

no.	Pressure	$(\frac{V}{V_0})$	Ref	no.	Pressure	$(\frac{V}{V_0})$	Ref
1	2.5	0.979	1	2	5.0	0.96	1
3	7.5	0.942	1	4	10.0	0.925	1
5	15.0	0.895	1	6	20.0	0.877	1
7	25.0	0.861	1	8	5.6	0.9471	2
9	8.1	0.9236	2	10	14.3	0.9064	2
11	17.9	0.8794	2	12	22.1	0.8659	2
13	26.5	0.8451	2	14	36.6	0.8139	2
15	40.1	0.7988	2	16	49.7	0.7794	2
17	57.8	0.7562	2	18	65.2	0.7344	2
19	0.9	0.99	3	20	5.9	0.964	3
21	9.0	0.936	3	22	9.1	0.934	3
23	10.9	0.927	3	24	13.2	0.907	3
25	15.8	0.892	3	26	18.7	0.875	3
27	18.8	0.882	3	28	21.0	0.868	3
29	21.5	0.866	3	30	26.0	0.859	3
31	29.3	0.836	3	32	34.4	0.83	3
33	36.9	0.813	3	34	41.0	0.798	3
35	46.1	0.779	3	36	51.0	0.771	3
37	54.5	0.763	3	38	60.3	0.751	3
39	62.8	0.743	3	40	64.1	0.741	3
41	4.5	0.9682	4	42	10.1	0.9327	4

Continued on next page

Table A.2 – *Continued from previous page*

no.	Pressure	$(\frac{V}{V_0})$	Ref	no.	Pressure	$(\frac{V}{V_0})$	Ref
43	14.5	0.9058	4	44	19.3	0.8808	4
45	25.5	0.8554	4	46	31.8	0.8319	4
47	36.9	0.8172	4	48	42.7	0.7939	4
49	48.0	0.7813	4	50	52.2	0.7693	4
51	56.2	0.7572	4	52	59.2	0.7501	4
53	61.2	0.7461	4	54	8.0	0.937	5
55	21.9	0.869	5	56	42.0	0.788	5
57	54.3	0.757	5	58	60.0	0.744	5

[1] (Perezalbuerne & Drickamer 1965)
[2] (Speziale, Shieh & Duffy 2006)
[3] (Mammone, Mao & Bell 1981)
[4] (Yamanaka, Kittaka & Nagai 2002)
[5] (Richet, Mao & Bell 1988)

Table A.3: Experimental pressure-volume data for Al_2O_3 at T = 300 K

no.	Pressure	$(\frac{V}{V_0})$	Ref	no.	Pressure	$(\frac{V}{V_0})$	Ref
1	1.24	0.9948	1	2	2.24	0.9914	1
3	2.63	0.9891	1	4	4.35	0.9822	1
5	5.05	0.9799	1	6	6.69	0.9724	1
7	7.34	0.9704	1	8	7.61	0.9686	1
9	8.47	0.9655	1	10	8.88	0.964	1
11	9.13	0.9628	1	12	10.85	0.9571	1
13	12.08	0.9517	1	14	0.0001	1.0	2
15	0.88	0.9969	2	16	1.71	0.9929	2
17	2.5	0.989	2	18	3.25	0.9863	2

Continued on next page

Table A.3 – *Continued from previous page*

no.	Pressure	$(\frac{V}{V_0})$	Ref	no.	Pressure	$(\frac{V}{V_0})$	Ref
19	3.95	0.9835	2	20	5.24	0.9772	2
21	6.8	0.9721	2	22	0.0001	1.0	2
23	1.09	0.9965	2	24	2.06	0.9914	2
25	3.33	0.9847	2	26	4.36	0.9792	2
27	5.36	0.9764	2	28	6.3	0.98	3
29	12.8	0.96	3	30	19.2	0.94	3
31	25.6	0.92	3	32	28.8	0.91	3
33	30.4	0.905	3	34	2.8	0.991	4
35	4.2	0.983	4	36	6.0	0.979	4
37	7.4	0.973	4	38	8.1	0.971	4
39	9.0	0.967	4	40	9.0	0.9651	5
41	15.6	0.9504	5	42	21.6	0.937	5
43	26.3	0.9166	5	44	32.6	0.9085	5
45	33.7	0.9024	5	46	41.3	0.8902	5
47	45.6	0.878	5	48	49.3	0.8714	5
49	21.29	0.9416	6	50	21.3	0.9416	6
51	23.22	0.9366	6	52	23.04	0.9346	6
53	22.47	0.9316	6	54	30.54	0.9125	6
55	31.83	0.9145	6	56	31.71	0.9135	6
57	35.52	0.9054	6	58	35.49	0.9054	6
59	47.54	0.8783	6	60	48.8	0.8763	6
61	49.32	0.8712	6	62	50.68	0.8702	6
63	50.63	0.8692	6	64	54.2	0.8612	6
65	55.72	0.8622	6	66	58.85	0.8511	6
67	59.67	0.8531	6	68	60.77	0.8511	6

Continued on next page

Table A.3 – *Continued from previous page*

no.	Pressure	$(\frac{V}{V_0})$	Ref	no.	Pressure	$(\frac{V}{V_0})$	Ref
69	66.63	0.8431	6	70	66.14	0.8391	6
71	66.15	0.837	6	72	66.14	0.837	6
73	72.93	0.831	6	74	72.92	0.831	6
75	76.46	0.825	6	76	76.11	0.822	6
77	77.84	0.82	6	78	78.77	0.8189	6
79	78.78	0.82	6	80	84.01	0.821	6
81	94.51	0.8029	6	82	97.2	0.8019	6
83	98.17	0.7978	6	84	98.42	0.7898	6
85	109.3	0.7767	6	86	106.1	0.7707	6
87	108.6	0.7737	6	88	112.5	0.7767	6
89	119.2	0.7627	6	90	118.8	0.7607	6
91	118.6	0.7576	6	92	119.7	0.7587	6
93	126.8	0.7637	6	94	127.4	0.7617	6
95	133.6	0.7486	6	96	133.3	0.7466	6
97	132.6	0.7376	6	98	136.4	0.7426	6
99	144.8	0.7416	6	100	143.5	0.7376	6

[1] (Sato & Akimoto 1979)
[2] (Grevel, Burchard, Fasshauer & Peun 2000)
[3] (Hart & Drickamer 1965)
[4] (d'amour, Schiferl, Denner, Schulz & Holzapfel 1978)
[5] (Richet, Xu & Mao 1988)
[6] (Marsh 1980)

Table A.4: Experimental pressure-volume data for SiO_2(α-quartz) at T = 300 K

no.	Pressure	$(\frac{V}{V_0})$	Ref	no.	Pressure	$(\frac{V}{V_0})$	Ref
1	2.0	0.945	1	2	5.1	0.8902	1
3	8.0	0.8548	1	4	9.5	0.8404	1
5	12.5	0.8145	1	6	15.3	0.7881	1
7	3.38	0.9309	2	8	4.88	0.9076	2
9	4.99	0.9083	2	10	5.92	0.8912	2
11	6.61	0.8829	2	12	6.65	0.8844	2
13	7.55	0.8765	2	14	8.36	0.8646	2
15	9.12	0.8586	2	16	9.69	0.8526	2
17	9.69	0.8517	2	18	10.18	0.8459	2
19	10.21	0.846	2	20	11.09	0.8378	2
21	12.07	0.832	2	22	4.54	0.922	3
23	5.58	0.905	3	24	8.56	0.857	3
25	9.43	0.845	3	26	9.57	0.842	3
27	9.68	0.839	3	28	9.8	0.836	3
29	10.2	0.829	3	30	9.91	0.836	3
31	2.07	0.9568	4	32	3.1	0.9304	4
33	3.76	0.9247	4	34	4.86	0.9075	4
35	5.58	0.8991	4	36	6.14	0.8897	4

[1] (Hazen, Finger, Hemley & Mao 1989)
[2] (Olinger & Halleck 1976)
[3] (Wackerle 1962)
[4] (Levien, Prewitt & Weidner 1980)

Table A.5: Experimental pressure-volume data for NaCl at T = 300 K

no.	Pressure	$(\frac{V}{V_0})$	Ref	no.	Pressure	$(\frac{V}{V_0})$	Ref
1	3.0	0.904	1	2	12.0	0.76	1
3	20.0	0.702	1	4	20.0	0.699	1
5	22.0	0.697	1	6	25.0	0.675	1
7	29.0	0.658	1	8	34.0	0.636	1
9	37.0	0.628	1	10	2.5	0.918	2
11	5.0	0.864	2	12	7.5	0.823	2
13	10.0	0.792	2	14	15.0	0.742	2
15	20.0	0.702	2	16	25.0	0.67	2
17	3.35	0.8982	3	18	3.85	0.8879	3
19	4.55	0.8732	3	20	5.7	0.8515	3
21	8.95	0.8028	3	22	13.1	0.7564	3
23	13.4	0.7538	3	24	17.25	0.7208	3
25	23.1	0.6809	3	26	25.7	0.6662	3
27	26.5	0.6621	3	28	29.15	0.6492	3
29	30.0	0.6452	3	30	30.6	0.642	3
31	30.85	0.6409	3	32	32.4	0.6339	3
33	35.0	0.6241	3	34	1.0	0.9627	4
35	2.0	0.9324	4	36	3.0	0.9067	4
37	4.0	0.8845	4	38	5.0	0.8649	4
39	10.0	0.791	4	40	15.0	0.7397	4
41	20.0	0.7004	4	42	25.0	0.6685	4
43	30.0	0.6416	4	44	2.895	0.918	5
45	3.541	0.903	5	46	3.843	0.901	5
47	3.934	0.893	5	48	5.451	0.878	5
49	5.431	0.865	5	50	5.656	0.862	5

Continued on next page

Table A.5 – *Continued from previous page*

no.	Pressure	$(\frac{V}{V_0})$	Ref	no.	Pressure	$(\frac{V}{V_0})$	Ref
51	5.866	0.851	5	52	5.991	0.849	5
53	5.981	0.848	5	54	7.461	0.83	5
55	7.438	0.829	5	56	7.837	0.828	5
57	7.662	0.824	5	58	8.017	0.824	5
59	8.871	0.82	5	60	11.09	0.791	5
61	10.98	0.787	5	62	11.55	0.786	5
63	11.7	0.782	5	64	11.77	0.773	5
65	11.85	0.775	5	66	12.05	0.776	5
67	12.15	0.776	5	68	12.09	0.774	5
69	12.21	0.775	5	70	12.19	0.769	5
71	13.13	0.757	5	72	13.11	0.757	5
73	13.07	0.755	5	74	16.87	0.734	5
75	17.21	0.738	5	76	16.94	0.734	5
77	17.15	0.735	5	78	18.45	0.727	5
79	18.03	0.717	5	80	17.99	0.716	5
81	19.25	0.723	5	82	21.46	0.709	5
83	22.46	0.705	5	84	22.54	0.696	5
85	22.8	0.692	5	86	23.4	0.693	5
87	23.66	0.692	5	88	25.36	0.686	5
89	25.38	0.687	5	90	25.89	0.683	5
91	25.87	0.683	5	92	26.01	0.68	5
93	26.05	0.679	5	94	26.38	0.683	5
95	26.8	0.677	5	96	26.74	0.675	5
97	26.79	0.675	5	98	26.98	0.674	5
99	27.57	0.673	5	100	27.67	0.668	5

Continued on next page

Table A.5 – *Continued from previous page*

no.	Pressure	$(\frac{V}{V_0})$	Ref	no.	Pressure	$(\frac{V}{V_0})$	Ref
101	27.59	0.666	5	102	28.12	0.666	5
103	28.26	0.668	5	104	28.22	0.667	5
105	28.78	0.659	5	106	29.52	0.66	5
107	29.32	0.655	5	108	29.3	0.651	5
109	30.57	0.654	5	110	30.18	0.646	5
111	30.64	0.645	5	112	32.9	0.63	5
113	33.27	0.62	5				

[1] (Sato-Sorensen 1983)
[2] (Perezalbuerne & Drickamer 1965)
[3] (Liu & Basset 1973)
[4] (Birch 1986)
[5] (Marsh 1980)

Table A.6: Experimental pressure-volume data for $MgCO_3$ at T = 300 K

no.	Pressure	$(\frac{V}{V_0})$	Ref	no.	Pressure	$(\frac{V}{V_0})$	Ref
1	0.3	0.9985	1	2	0.74	0.9945	1
3	1.39	0.9888	1	4	1.75	0.9858	1
5	1.93	0.9838	1	6	2.26	0.9818	1
7	2.34	0.9807	1	8	2.71	0.9778	1
9	3.09	0.9751	1	10	3.34	0.9728	1
11	3.7	0.9699	1	12	4.02	0.9677	1
13	4.16	0.9675	1	14	4.77	0.9629	1
15	5.61	0.9556	1	16	6.05	0.9521	1
17	6.42	0.95	1	18	6.88	0.9464	1
19	1.9	0.9846	2	20	3.0	0.9734	2

Continued on next page

Table A.6 – *Continued from previous page*

no.	Pressure	$(\frac{V}{V_0})$	Ref	no.	Pressure	$(\frac{V}{V_0})$	Ref
21	4.2	0.9633	2	22	6.1	0.9517	2
23	7.7	0.9382	2	24	9.1	0.9271	2
25	9.9	0.9252	2	26	10.8	0.9208	2
27	12.3	0.9132	2	28	14.0	0.9033	2
29	16.0	0.8909	2	30	17.8	0.8832	2
31	19.0	0.8779	2	32	21.0	0.8687	2
33	23.3	0.8617	2	34	25.6	0.8539	2
35	27.1	0.8479	2	36	15.4	0.8965	2
37	19.9	0.8753	2	38	28.3	0.8423	2
39	33.0	0.8253	2	40	39.7	0.8063	2
41	0.14	1.001	2	42	0.78	0.9942	2
43	2.0	0.9832	2	44	3.3	0.9735	2
45	5.0	0.9622	2	46	7.2	0.9502	2
47	9.34	0.9351	2	48	9.6	0.9354	2
49	10.8	0.9303	2	50	14.0	0.9135	2
51	16.8	0.8966	2	52	19.9	0.8878	2
53	15.9	0.9039	2	54	13.0	0.9223	2
55	0.81	0.9937	2	56	0.41	0.9967	2
57	1.28	0.9855	2	58	2.05	0.9801	2
59	3.74	0.9664	2	60	5.6	0.9586	2
61	7.03	0.9424	2	62	9.0	0.931	2
63	11.7	0.9179	2	64	14.7	0.8963	2
65	18.9	0.8846	2	66	25.1	0.8528	2

[1] (Ross 1997)
[2] (Fiquet & Reynard 1999)

Appendix B

Matlab code

In this appendix some selected Matlab scripts for the calculations performed has been given. The selection is done such that scripts with identical functionality, and which differ only in what solids they handle, are listed just once. The complete set of Matlab scripts for all the solids has been attached as a zip file. Where there is individual scripts for each solid MgO has been chosen as an example.

B.1 Data management

The following script shows how the data is prepared for use in the forthcoming calculations for MgO.

```
% Transforming the data into a coloumn vector consisting of V/V0 and
% pressure p, i.e. [VdivV0',p,]'. It also returns the length of each
% dataset

function [p, VdivV0, len] = pvdata_mgo()

h1 = load('Speziale_Zha_etal_2001.txt');
h2 = load('Mao_Bell_1979.txt');
h3 =load('PerezAlbuerne_Drickamer_1965.txt');
h4 =load('Li_Woody_etal_2006.txt');
h5 =load('Jacobsen_Holl_etal_2008a.txt');
h6 =load('Jacobsen_Holl_etal_2008b.txt');
h7 =load('Jacobsen_Holl_etal_2008c.txt');
h8 = load('LASL.txt');
```

```
numDatasets = 8;

% Transforming into V/V0 since the data is given in V in some papers
%--------------------------------------------------------------------------
VdivV02 = zeros(length(h1(:,3)),1);
for i = 1:1:length(h1(:,3))
VdivV02(i,1) = h1(i,3)/74.71; % 74.71 where given as V0 in Speziale..
end

VdivV03 = zeros(length(h5(:,3)),1);
for i = 1:1:length(h5(:,3))
VdivV03(i,1) = h5(i,3)/74.698;
end

VdivV04 = zeros(length(h6(:,3)),1);
for i = 1:1:length(h6(:,3))
VdivV04(i,1) = h6(i,3)/74.698;
end

VdivV05 = zeros(length(h7(:,3)),1);
for i = 1:1:length(h7(:,3))
VdivV05(i,1) = h7(i,3)/74.698;
end

%--------------------------------------------------------------------------
% Combining into two vectors of p and VdivV0
p     = [h1(:,2)',h2(:,2)',h3(:,2)',h4(:,2)', h5(:,2)',...
     h6(:,2)',h7(:,2)',h8(:,2)']';
gamma = 0.928/0.915;
h8(:,3)=h8(:,3).^gamma;
VdivV0 = [VdivV02', h2(:,3)',h3(:,3)',h4(:,3)', ...
          VdivV03', VdivV04',VdivV05', h8(:,3)']';

%--------------------------------------------------------------------------
% Making a vector which contains the length of the different datasets
len = zeros(1,numDatasets);

len(1)        = length(h1(:,2));
len(2)        = length(h2(:,2));
len(3)        = length(h3(:,2));
len(4)        = length(h4(:,2))+length(h5(:,2))+length(h6(:,2));
len(5)        = length(h7(:,2));
len(6)        = length(h8(:,2));

%--------------------------------------------------------------------------
```

B.2 Implementation of the second order Murnaghan on implicit form

The implementation of the implicit second order Murnaghan equation of state is given in the following script.

```
% Nonlinear least squares for a fitting curve on the form
% log(V/V0) + 1/(K01*(a-b))*log((1+a*p)/(1+b*p)) = 0
% Here, x vector is [K01; K02; K03]
% xdata is the reduced volume and pressure
% param is the extra input as a struct, accessed by param(1).xxxx

function [F, means] = newcurve_res_mgo(x, xdata, param)

K01 = x(1);
K02 = x(2);
K03 = x(3);
n = length(xdata)/2;
m = length(xdata);
a = K02/(2*K01)*(1+sqrt(1-4*K03*K01/(K02^2)));
b = K02/K01-a;
F = log(xdata(1:n))+ 1/(K01*(a-b))*log((1+a*xdata(n+1:m))./(1+b*xdata(n+1:
    m)));

% Finding the mean for each experimental series
means = zeros(1,length(param.len)-1);

% Making the final matrix to be returned
F = [F;zeros(size(F))];
```

B.3 Parameter fitting

The following script shows how the nonlinear regression has been used to find the optimal parameters. MgO has been chosen as an example.

```
% Nonlinear least squares with use of matlab's lsqcurvefit
% ydata is here zeros and xdata is the V/V0 and p

function K = lsq_mgo()
clear all
clc
close all
```

```
x0 = [160 4 -0.02]; % Guesses

[p, VdivV0,len] = pvdata_mgo();
xdata = [VdivV0', p']';
ydata = zeros(size(xdata));
n = length(xdata)/2;
m = length(xdata);
%-------------------------------------------------------------------------
% Making a vector, len2, which contains the number of measuring points in
% each series
len2 = zeros(1, length(len)+1);
for i = 2:length(len2)
  len2(i) = sum(len(1:i-1));
end

% Gives the extra option parameters, param, through a struct array
param = struct('len', len2);
f = @(x,xdata)newcurve_res_mgo(x,xdata,param);

% Calling the function lsqcurvefit
[x,error] = lsqcurvefit(f,x0,xdata,ydata);
disp(error)
fprintf('K01 =%g;\n', x(1));
fprintf('K02 =%g;\n', x(2));
fprintf('K03 =%g;\n', x(3));
K = x;

%-------------------------------------------------------------------
% Plotting the residual plot and getting the mean for each series
[F, mean] = newcurve_res_mgo(x, xdata,param);
subplot(2,1,1)

% Plotting all the experimental series
marker = ['*', 'p', 'o', '+', 'x', 's', 'd', 'v']';
hold on
for i = 1:length(len2)-1
plot(xdata(n+1+len2(i):n+len2(i+1)), F(1+len2(i):len2(i+1)), marker(i))
end
hold off

%-----------------------------------------------------------------
% Making a contour plot for K02 and K03 to find if a minimum exists, and
    if
% so where it exists
K01 = x(1);
K02 = linspace(-1.3305,7.2901,500);
```

```
K03 = linspace(-0.022,0.0408,500);
Y = zeros(length(K02), length(K03));
for i = 1:length(K02)
    for j = 1:length(K03)
        k02 = K02(i);
        k03 = K03(j);
        a = k02/(2*K01)*(1+sqrt(1-4*k03*K01/(k02^2)));
        b = k02/K01-a;
        y = (log(xdata(1:n)) + 1/(K01*(a-b))*log((1+a*xdata(n+1:m))./(1+b*
            xdata(n+1:m))));
        Y(i,j) = sqrt(y'*y);
    end
end
Y(Y>3*min(min(Y))) = NaN;

% Plotting the contour plot
figure(2)
vector2 = 0:0.002:0.01;
contour(K03,K02,Y-min(min(Y)),vector2)
% title('Contour plot for MgO')
xlabel('K_0''''')
ylabel('K_0''')

figure(3)
plot(p, VdivV0, '*');
%-------------------------------------------------------------------
```

B.4 The bootstrap method

The bootstrap method for finding standard deviation is shown in the following script.

```
% Bootstrapping of data
clc
clear all
close all

% Getting the data for the solids, choose the path that is wanted
% and change the names for lsq and pvdata accordingly
% addpath('Al2O3')
addpath('MgO')
% addpath('NaCl')
% addpath('SiO2')
% addpath('CaO')
% addpath('MgCO3')
```

```
14
15 % The optimal values calculated from lsq
16
17 theta_opts = lsq_mgo();
18 close all
19
20 x0 = theta_opts; % Guesses for parameters
21
22 [p, VdivV0, len] = pvdata_mgo();
23 xdata = [VdivV0'; p']';
24 % xdata = [[VdivV0',VdivV0'];[p',p']]';
25 xdata2 = [VdivV0',p']';
26
27 nl = length(xdata)/2;
28 m = length(xdata);
29 %-------------------------------------------------------------------------
30 % Making a vector, len2, which contains the number of measuring points in
31 % each series
32 len2 = zeros(1, length(len)+1);
33 for i = 2:length(len2)
34   len2(i) = sum(len(1:i-1));
35 end
36
37 % Gives the extra option parameters, param, through a struct array
38 param = struct('len', len2);
39 %-------------------------------------------------------------------------
40 n = length(xdata);        %size of each data set
41 nReps = 2000;  %number of data sets or 'experiments'
42 % myStat = @mean; % function handle which gives mean
43 id = randi(n,n,nReps);
44 bootstrapData = zeros(n,2,nReps); % size 220, 2, 2000
45 for i = 1:nReps
46    bootstrapData(:,:,i) = xdata(id(:,i),:); % Gives all the different
47 end                                          %bootstrapdata
48
49
50 xdata_new = zeros(2*n,1);
51 ydata = zeros(size(xdata_new));
52 x = zeros(nReps,length(x0));
53 for i = 1:nReps
54     xdata_new = bootstrapData(:,:,i);
55     xdata_f   = [xdata_new(:,1)',xdata_new(:,2)']; % Rearranging
56     f = @(x,xdata)residual(x,xdata,param);          % to getting
57     x(i,:) = lsqcurvefit(f,x0,xdata_f,ydata);       % the correct form
58 end
59
```

```
for i = 1:length(x)
    if imag(x(i,:))~= 0
        x(i,1)=theta_opts(1);
        x(i,2)=theta_opts(2);
        x(i,3)=theta_opts(3);
    end
end
theta_opt = zeros(nReps, length(x0));
for i = 1:nReps
  theta_opt(i,:)=theta_opts;
end
% cov(theta)=E[(theta-theta_opt)(theta-theta_opt)']
covtheta = zeros(3,3);
covtheta(1,1) = mean((x(:,1)-theta_opt(:,1)).*((x(:,1)-theta_opt(:,1))));
covtheta(1,2) = mean((x(:,1)-theta_opt(:,1)).*((x(:,2)-theta_opt(:,2))));
covtheta(1,3) = mean((x(:,1)-theta_opt(:,1)).*((x(:,3)-theta_opt(:,3))));
covtheta(2,1) = mean((x(:,2)-theta_opt(:,2)).*((x(:,1)-theta_opt(:,1))));
covtheta(2,2) = mean((x(:,2)-theta_opt(:,2)).*((x(:,2)-theta_opt(:,2))));
covtheta(2,3) = mean((x(:,2)-theta_opt(:,2)).*((x(:,3)-theta_opt(:,3))));
covtheta(3,1) = mean((x(:,3)-theta_opt(:,3)).*((x(:,1)-theta_opt(:,1))));
covtheta(3,2) = mean((x(:,3)-theta_opt(:,3)).*((x(:,2)-theta_opt(:,2))));
covtheta(3,3) = mean((x(:,3)-theta_opt(:,3)).*((x(:,3)-theta_opt(:,3))));

[Q2,L2] = eig(covtheta);
F = returnf(x0,xdata2);
s2 = 1/((length(F)-length(x0)))*(F'*F); % Residual sum of squares

B = Q2*sqrt(L2);

Imat = inv(B)*Q2*L2*Q2'*inv(B)';

k = x*(Q2*diag(1./(sqrt(diag(L2)))));
k_opt = theta_opt*(Q2*diag(1./(sqrt(diag(L2)))));
covkappa = zeros(3,3);
covkappa(1,1) = mean((k(:,1)-k_opt(:,1)).*((k(:,1)-k_opt(:,1))));
covkappa(1,2) = mean((k(:,1)-k_opt(:,1)).*((k(:,2)-k_opt(:,2))));
covkappa(1,3) = mean((k(:,1)-k_opt(:,1)).*((k(:,3)-k_opt(:,3))));
covkappa(2,1) = mean((k(:,2)-k_opt(:,2)).*((k(:,1)-k_opt(:,1))));
covkappa(2,2) = mean((k(:,2)-k_opt(:,2)).*((k(:,2)-k_opt(:,2))));
covkappa(2,3) = mean((k(:,2)-k_opt(:,2)).*((k(:,3)-k_opt(:,3))));
covkappa(3,1) = mean((k(:,3)-k_opt(:,3)).*((k(:,1)-k_opt(:,1))));
covkappa(3,2) = mean((k(:,3)-k_opt(:,3)).*((k(:,2)-k_opt(:,2))));
covkappa(3,3) = mean((k(:,3)-k_opt(:,3)).*((k(:,3)-k_opt(:,3))));

% disp(covkappa);

```

```
dtheta = zeros(3,3);
dtheta(:,1)=B*(k_opt(1,:)+[1 0 0])'-theta_opt(1,:)';
dtheta(:,2)=B*(k_opt(1,:)+[0 1 0])'-theta_opt(1,:)';
dtheta(:,3)=B*(k_opt(1,:)+[0 0 1])'-theta_opt(1,:)';

fprintf('std1 = [%f; %f; %f];\n',dtheta(1,1),dtheta(2,1) , dtheta(3,1))
fprintf('std2 = [%f; %f; %f];\n',dtheta(1,2),dtheta(2,2) , dtheta(3,2))
fprintf('std3 = [%f; %f; %f];\n',dtheta(1,3),dtheta(2,3) , dtheta(3,3))

%-----------------------------------------------------------------------
% Making a contour plot for K02 and K03 to find if a minimum exists, and
    if
% so where it exists
K01 = k_opt(1);
K02 = linspace(145,400,100);
K03 = linspace(-25,-150,100);
Y = zeros(length(K02), length(K03));
for i = 1:length(K02)
    for j = 1:length(K03)
        k01 = B(1,:)*[K01;K02(i);K03(j)];
        k02 = B(2,:)*[K01;K02(i);K03(j)];
        k03 = B(3,:)*[K01;K02(i);K03(j)];
        a = k02/(2*k01)*(1+sqrt(1-4*k03*k01/(k02^2)));
        b = k02/k01-a;
        y = (log(VdivV0) + 1/(k01*(a-b))*log((1+a*p)./(1+b*p)));
        Y(i,j) = sqrt(y'*y);
    end
end
Y(Y>3*min(min(Y))) = NaN;

% Plotting the contour plot
% subplot(2,1,2)
figure(4)
vector2 = 0:0.02:0.1;
contour(K03,K02,Y-min(min(Y)),vector2)
% title('Contour plot for MgO')
xlabel('\kappa{}_3')
ylabel('\kappa{}_2')
```

B.5 Deviation plots

The calculation and plotting of the deviation plots are shown in the following script.

```
% Test of bulk modulus for the four different isothermal EOS
```

```
% versus the second order Murnaghan with uncertainty

clc
clear all
close all

V_V0 = 0.1:0.0001:1;
X = (V_V0).^(1/3);
scale = linspace(-3,3,1000);
Nsolids = 6;

% Values given for MgCO3 from lsq and firstdiff
t1='MgCO_3';
K1(1) =112.436;
K2(1) =4.76634;
K3(1) =-0.0270562;
std1(1,:) = [0.000043; 0.000440; 0.007388];
std2(1,:) = [0.115360; 0.429741; -0.026252];
std3(1,:) = [-3.049675; 0.816764; -0.030929];
pmaxi(1,:) = 39.7*ones(1,length(scale));

% Values given for NaCl from lsq and firstdiff
t2 = 'NaCl';
K1(2) =24.3804;
K2(2) =4.99712;
K3(2) =-0.0486765;
std1(2,:) = [0.000025; 0.000157; 0.002096];
std2(2,:) = [0.035737; 0.086438; -0.006905];
std3(2,:) = [-0.896211; 0.369168; -0.017092];
pmaxi(2,:) = 37*ones(1,length(scale));


% Values given for SiO2 from lsq
t3 = 'SiO_2';
K1(3) =38.5545;
K2(3) =5.44556;
K3(3) =-0.155289;
std1(3,:) = [0.000913; 0.003420; 0.021745];
std2(3,:) = [0.214945; 0.376384; -0.068223];
std3(3,:) = [-2.995555; 1.685451; -0.139257];
pmaxi(3,:) = 15.3*ones(1,length(scale));

% Values given for CaO from lsq
t4 = 'CaO';
K1(4) =109.401;
K2(4) =4.92936;
```

```
K3(4) =-0.0276964;
std1(4,:) = [0.000002; 0.000030; 0.000988];
std2(4,:) = [0.026185; 0.182513; -0.005618];
std3(4,:) = [-4.898921; 0.702416; -0.013587];
pmaxi(4,:) = 65.2*ones(1,length(scale));

% Values given for Al2O3 from lsq
t5 = 'Al_2O_3';
K1(5) =269.773;
K2(5) =4.35411;
K3(5) =-0.0130543;
std1(5,:) = [0.000000; 0.000012; 0.000784];
std2(5,:) = [0.009872; 0.154277; -0.002390];
std3(5,:) = [-9.097483; 0.582079; -0.005196];
pmaxi(5,:)=144.7670*ones(1,length(scale));

% Values given for MgO from lsq
t6 = 'MgO';
K1(6) =160.123;
K2(6) =3.93044;
K3(6) =-0.00269764;

std1(6,:) = [0.000001; 0.000021; 0.000802];
std2(6,:) = [0.008561; 0.076362; -0.002009];
std3(6,:) = [-2.421412; 0.371368; -0.003795];
pmaxi(6,:) = 121.752*ones(1,length(scale));

%-------------------------------------------------------------------------
% Calculating the parameters with standard deviation
%-------------------------------------------------------------------------
titles = {t1, t2, t3, t4, t5, t6};

for i = 1:Nsolids
figure(i)
std = [std1(i,:);std2(i,:);std3(i,:)];
% std = abs(std);
K01 = K1(i);
K02 = K2(i);
K03 = K3(i);
pmax = pmaxi(i,:);
title(titles(i));
%-------------------------------------------------------------------------

%Murnaghan
K_Mur = K01*X.^(-3*K02);
p_Mur = K01/K02*(X.^(-3*K02)-1);
```

```
94
95 %Birch-Murnaghan
96 K_Bir = 0.5*K01*(7*X.^(-7)-5*X.^(-5))+3/8*K01*(K02-4)*(9*X.^(-9)-14*X
       .^(-7)+5*X.^(-5)); %Checked
97 p_Bir = 3/2*K01*(X.^(-7)-X.^(-5)).*(1+3/4*(K02-4)*(X.^(-2)-1));
98
99 %Vinet
100 K_Vin = K01*X.^(-2).*(1+(3/2*(K02-1)*X + 1).*(1-X)).*exp(3/2*(K02-1)*(1-X)
       );
101 p_Vin = 3*K01*(1-X)./(X.^2).*exp(3/2*(K02-1)*(1-X));
102
103 %Pseudo-Spinodal
104 beta = 0.85;
105 A = beta*K01/K02;
106 B = K01*(1-beta);
107 C = A^beta;
108 D = 1/(1-beta);
109 p_Spi = (((A-log(V_V0)*B)/C).^(D))-A;
110
111 kappa = (A^beta)/K01;
112 E = beta/((1-beta)*K02);
113 F = kappa/(1-beta);
114 pspi = (((E-log(V_V0))/F).^D) - A;
115 K_Spi = 1/kappa*(pspi+A).^beta;
116
117 % Our equation
118 a = K02/(2*K01)*(1+sqrt(1-4*K03*K01/(K02^2)));
119 b = K02/K01-a;
120 c = K01*(a-b);
121 p_Our = 0:1:500;
122 K_Our = K01 + K02*p_Our + K03/2*p_Our.^2;
123 Y_Our    = ((K_Our - K02*p_Our)/K01)';
124
125 % Making residuals
126 Y_Mur = (K_Mur - K02*p_Mur)/K01*1.0000000000001;% Remove roughness
127 Y_Bir = (K_Bir - K02*p_Bir)/K01;
128 Y_Vin = (K_Vin - K02*p_Vin)/K01;
129 Y_Spi = (K_Spi - K02*p_Spi)/K01;
130
131 % Plotting
132 colors = [([0.75 0.75 0.75]);([0.8 0.8 0.8]);([0.65 0.65 0.65])];
133 location = [([.4,.7,.4,.2]);([.47,.48,.4,.2]);([.47,.48,.4,.2])
       ;([.43,.7,.4,.2]);([.17,.15,.4,.2]);([.165,.15,.4,.2])]; %([left,
       bottom,width,height])
134 axis([0 200 -3 3])
135 xlabel('Pressure [GPa]')
```

```
ylabel('(K - (K_0''p))/K01 [-]')
hold on
for j = 1:length(std)
stdK01=std(j,1);
stdK02=std(j,2);
stdK03=std(j,3);
K01_u = K01 + stdK01;
K02_u = K02 + stdK02;
K03_u = K03 + stdK03;
K01_l = K01 - stdK01;
K02_l = K02 - stdK02;
K03_l = K03 - stdK03;
K_Our_u = K01_u + K02_u*p_Our + K03_u/2*p_Our.^2;
K_Our_l = K01_l + K02_l*p_Our + K03_l/2*p_Our.^2;
Y_Our_u = ((K_Our_u - K02*p_Our)/K01)';
Y_Our_l = ((K_Our_l - K02*p_Our)/K01)';
Y_Our_p = max(Y_Our_u,Y_Our_l);
Y_Our_m = min(Y_Our_u,Y_Our_l);
h1 =jbfill(p_Our,Y_Our_p',Y_Our_m',[0.6 0.8 0.8]);
end

hold on
axis([0 200 -2 2])

h3 = plot(p_Mur,Y_Mur, 'color',[0,0.8,0],'LineWidth',1.5);
h4 = plot(p_Bir,Y_Bir, 'b','LineWidth',1.5);
h5 = plot(p_Vin,Y_Vin, 'r','LineWidth',1.5);
h6 = plot(p_Spi,Y_Spi, 'magenta','LineWidth',1.5);
h7 = plot(pmax,scale, '--black');
h_legend = legend([h1, h3, h4, h5, h6, h7],...
    {'Second order Murnaghan with uncertainty','Murnaghan', 'Birch', '
        Vinet', 'Pseudo-spinodal', 'Maximum experimental pressure'});
set(h_legend,'FontSize',8,'Position',location(i,:));
filename=sprintf('bulk%g.svg',i);
plot2svg(filename)

hold off
end
```

B.6 Isobaric heat capacity as a function of temperature

The prediction of isobaric heat capacity as a function of temperature for MgO has been shown in the following script.

```
% MgO heat capacity as a function of temperature
clear all
close all
clc

% MgO
K01 =160.123e9; % Pa = J/m^3
K02 =3.93;
V0 = 11.25e-6; % m^3/mol
gamma0 = 1.49; % Speziale 2001
theta = 743*0.75;
N = 2*6.023*10^-23;
Tref = 298;
Mw = 40.31;

beta = 0.85;
kb = 1.38e23;
pres = [0.0001 5 10 20 30]*10^9;

%-------------------------------------------------------------------------
% Data from JANAF
A = 47.25995;
B = 5.681621;
C = -0.872665;
D = 0.104300;
E = -1.053955;
TJA = (298:1:3050);
TJ = TJA/1000;
CpJanaf = A + B*TJ + C*(TJ.^2) + D*(TJ.^3) + E./(TJ.^2);
%-------------------------------------------------------------------------
% Experimental heat capacity
addpath(cd('..\'));
h1 = load('barron_and_berg_etal_1959_cp.txt');
cp1 = h1(:,3)*4.184;
Texp = h1(:,2);
Cpexp = cp1;

%-------------------------------------------------------------------------
T = [Texp;TJA'];
colors = char('blue','r','cyan','green','magenta');
marker = char('d');
for i = 1:length(pres)
p = pres(i);
psp298 = -K01/K02*0.85;
psp0 = psp298 - (gamma0/V0*3*N*kb*theta*(0.5+1./(exp(theta./Tref)-1)));
pspTref = psp0 + (gamma0/V0*3*N*kb*theta*(0.5+1./(exp(theta./Tref)-1)));
```

```
ha = (gamma0/V0*3*N*kb*theta*(0.5+1./(exp(theta./T)-1)));
psp = psp0 + ha;
kappa = ((-pspTref).^beta)/K01; % Utregna ved Tref, independent of T

K_spi  = (1./kappa).*(p-psp).^beta; % Bulk modulus
K_spi2 = (beta./kappa).*(p-psp).^(beta-1); % pressure deriv, bulk modulus

a = (gamma0./(V0.*K_spi)*3*N*kb.*((theta./T).^2)).*exp(theta./T)./((exp(
    theta./T)-1).^2); % K^-1
Cpps = (3*N*kb.*((theta./T).^2)).*exp(theta./T)./((exp(theta./T)-1).^2)
    .*(1+T.*a.*gamma0);

Vsp = V0.*exp(beta./((1-beta)*K02)); % Vsp is evaluated at reference state
V01 = Vsp*exp(-kappa/(1-beta).*(-psp).^(1-beta)); % V(p=0)
V = Vsp.*exp(-kappa/(1-beta)*(p-psp).^(1-beta));

% Chemical potential
k = kappa;
a2 = -k/(1-beta);
b = psp;
c = 1-beta;
p0 = 0;
my1 = (b-p).*(-a2.*(p-b).^c).^(-1/c);
myg = (gammainc(-a2.*(p-b).^c,1/c,'upper')).*gamma(1/c);
my = Vsp.*my1.*myg./c;

my10 = (b-p0).*(-a2*(p0-b).^c).^(-1/c);
myg0 = (gammainc(-a2*(p0-b).^c,1/c,'upper'))*gamma(1/c);
my0 = Vsp.*my10.*myg0./c;

mytot  = my-my0; % J/mol
mym    = my*Mw;  % J/g
mytotm = mytot*Mw;%J/g

d1 = central_diff(mytot,T);
d2 = central_diff(d1,T);
%--------------------------------------------------------------------
% Plotting
hp = figure(1);
hold on
xlabel('Temperature [K]','fontsize',10)
ylabel('C_p [J/(K, mol)]','fontsize',10)
Cpcalc1 = -Texp.*d2(1:length(Texp))+Cpexp;
Cpcalc2 = -TJA'.*d2(length(Texp)+1:end)+CpJanaf';
h1(i)=plot(Texp,Cpcalc1, marker);
h2(i)=plot(TJA',Cpcalc2);
```

```
set(h1(i),'color', colors(i), 'MarkerSize', 4)
set(h2(i), 'color', colors(i), 'Linewidth', 1.5)
hAnnotation = get(h1(i),'Annotation');
hLegendEntry = get(hAnnotation','LegendInformation');
set(hLegendEntry,'IconDisplayStyle','off')
end

axis([0 3000 -20 60])
leg = legend('0.0001 GPa','1000 GPa','10 GPa','20 GPa','30 GPa');
set(leg,'Location','SouthEast','fontsize',10)
set(hp,'WindowStyle','docked')
set(gca,'fontsize',10)
set(hp,'PaperpositionMode','auto')
% saveas(1,'C:\Users\Stig-Erik\NTNU\Master\Latex\MgO_Cpexp','epsc')
```

B.7 Isobaric heat capacity as a function of pressure

The prediction of isobaric heat capacity as a function of pressure for MgO has been shown in the following script.

```
% MgO heat capacity as a function of pressure
clear all
close all
clc

% MgO
K01 =160.123e9; % Pa = J/m^3
K02 =3.93;
V0 = 11.25e-6; % m^3/mol
gamma0 = 1.49; % Speziale 2001
theta = 743*0.75;
N = 2*6.023*10^-23;
Tref = 298;
Mw = 40.31;

beta = 0.85;
kb = 1.38e23;
% T = (0:1:3000);
pres = [0.0001:5:220]*10^9;

%-------------------------------------------------------------------------
% Data from JANAF
A = 47.25995;
B = 5.681621;
```

```
C = -0.872665;
D = 0.104300;
E = -1.053955;
TJA = (298:1:3050);
TJ = TJA/1000;
CpJanaf = A + B*TJ + C*(TJ.^2) + D*(TJ.^3) + E./(TJ.^2);
%-------------------------------------------------------------------------
% Experimental heat capacity
addpath(cd('..\'));
h1 = load('barron_and_berg_etal_1959_cp.txt');
cp1 = h1(:,3)*4.184;
Texp = h1(:,2);
Cpexp = cp1;

%-------------------------------------------------------------------------
T = [Texp;TJA'];
colors = char('blue','r','cyan','green','magenta');
marker = char('d');
for i = 1:length(pres)
p = pres(i);
psp298 = -K01/K02*0.85;
psp0 = psp298 - (gamma0/V0*3*N*kb*theta*(0.5+1./(exp(theta./Tref)-1)));
pspTref = psp0 + (gamma0/V0*3*N*kb*theta*(0.5+1./(exp(theta./Tref)-1)));
ha = (gamma0/V0*3*N*kb*theta*(0.5+1./(exp(theta./T)-1)));
psp = psp0 + ha;
kappa = ((-pspTref).^beta)/K01; % Utregna ved Tref, independent of T

K_spi  = (1./kappa).*(p-psp).^beta; % Bulk modulus
K_spi2 = (beta./kappa).*(p-psp).^(beta-1); % pressure deriv, bulk modulus

a = (gamma0./(V0.*K_spi)*3*N*kb.*((theta./T).^2)).*exp(theta./T)./((exp(
    theta./T)-1).^2); % K^-1
Cpps = (3*N*kb.*((theta./T).^2)).*exp(theta./T)./((exp(theta./T)-1).^2)
    .*(1+T.*a.*gamma0);

Vsp = V0.*exp(beta./((1-beta)*K02)); % Vsp is evaluated at reference state
V01 = Vsp*exp(-kappa/(1-beta).*(-psp).^(1-beta)); % V(p=0)
V = Vsp.*exp(-kappa/(1-beta)*(p-psp).^(1-beta));

% Chemical potential
k = kappa;
a2 = -k/(1-beta);
b = psp;
c = 1-beta;
p0 = 0;
my1 = (b-p).*(-a2.*(p-b).^c).^(-1/c);
```

```
myg = (gammainc(-a2.*(p-b).^c,1/c,'upper')).*gamma(1/c);
my = Vsp.*my1.*myg./c;

my10 = (b-p0).*(-a2*(p0-b).^c).^(-1/c);
myg0 = (gammainc(-a2*(p0-b).^c,1/c,'upper'))*gamma(1/c);
my0 = Vsp.*my10.*myg0./c;

mytot  = my-my0; % J/mol
mym    = my*Mw;  % J/g
mytotm = mytot*Mw;%J/g

d1 = central_diff(mytot,T);
d2 = central_diff(d1,T);
%-------------------------------------------------------------------------
Cpcalc1 = -Texp.*d2(1:length(Texp))+Cpexp;
Cpcalc2 = -TJA'.*d2(length(Texp)+1:end)+CpJanaf';
Cpp1(i) = Cpcalc2(find(TJA==298));
Cpp2(i) = Cpcalc2(find(TJA==500));
Cpp3(i) = Cpcalc2(find(TJA==1000));
Cpp4(i) = Cpcalc2(find(TJA==2000));
Cpp5(i) = Cpcalc2(find(TJA==3000));

end
% Plotting
hp = figure(1);
hold on
xlabel('Pressure [GPa]','fontsize',12)
ylabel('C_p [J/(K, mol)]','fontsize',12)
axis([0 200 20 80])
plot(pres/10^9,Cpp1,colors(1),'linewidth',1.5)
plot(pres/10^9,Cpp2,colors(2),'linewidth',1.5)
plot(pres/10^9,Cpp3,colors(3),'linewidth',1.5)
plot(pres/10^9,Cpp4,colors(4),'linewidth',1.5)
plot(pres/10^9,Cpp5,colors(5),'linewidth',1.5)
leg = legend('298.15 K','500 K','1000 K','2000 K','3000 K');
set(leg,'Location','NorthEast','fontsize',10)
set(hp,'WindowStyle','docked')
set(gca,'fontsize',12)
set(hp,'PaperpositionMode','auto')
% saveas(1,'C:\Users\Stig-Erik\NTNU\Master\Latex\CpP_MgO','epsc')
```

B.8 Bulk modulus as a function of temperature

The prediction of the bulk modulus as a function of temperature for MgO has been shown in the following script.

```
% Pseudo-Spinodal equation
% Predictions for bulk modulus as a function of temperature for MgO

clear all
close all
clc

% MgO
K01 =160.123;
K02 =3.93;
V0 = 11.25; % cm^3/mol
gamma0 = 1.49; % Speziale 2001
theta = 743*0.75;
N = 2*6.023*10^-23;
Tref = 298;

beta = 0.85;
A = beta*K01/K02;
B = K01*(1-beta);
C = A^beta;
D = 1/(1-beta);
kb = 1.38*10^23;
T = (0:1:3000)';
pres = [0,5,10,20,30];
colors = char('blue','r','cyan','green','magenta');

for i = 1:length(pres)
p = pres(i);
psp298 = -K01/K02*0.85;
psp0 = psp298 - (gamma0/V0*3*N*kb*theta*(0.5+1./(exp(theta./Tref)-1)))
    /1000;
pspTref = psp0 + (gamma0/V0*3*N*kb*theta*(0.5+1./(exp(theta./Tref)-1)))
    /1000;
ha = (gamma0/V0*3*N*kb*theta*(0.5+1./(exp(theta./T)-1)))/1000;
psp = psp0 + ha;
kappa = ((-pspTref).^beta)/K01; % Calculated at Tref, independent of T
K_spi  = (1./kappa).*(p-psp).^beta; % Bulk modulus
K_spi2 = (beta./kappa).*(p-psp).^(beta-1); % Pressure derivative of
                                           % bulk modulus
Vsp = V0.*exp(beta./((1-beta)*K02));

```

```
V01 = Vsp*exp(-kappa/(1-beta).*(p-psp).^(1-beta));
V0T = Vsp*exp(-kappa/(1-beta).*(-psp).^(1-beta));
V0ref = Vsp*exp(-kappa/(1-beta).*(-pspTref).^(1-beta));

V = Vsp.*exp(-kappa/(1-beta)*(p-psp).^(1-beta));

VdivV0T = V/V0T;

a = (gamma0./(V0.*K_spi)*3*N*kb.*((theta./T).^2)).*exp(theta./T)./((exp(
    theta./T)-1).^2)/1000; % K^-1
%-------------------------------------------------------------------------
% Experimental data for alpha
h1 = load('anderson_and_zou_1989.txt');
Texp = h1(:,2);
alpha= h1(:,3)*10^-6;

%-------------------------------------------------------------------------
% Murnaghan
Kmur = K01+K02*p;
aMur = (gamma0./(V0.*Kmur)*3*N*kb.*((theta./T).^2)).*exp(theta./T)./((exp(
    theta./T)-1).^2)/1000;

% Calculating the isentropic bulk moduls
Ks = K_spi.*(1+a.*gamma0.*T);

% Plotting
size = 12;
hp = figure(1);
hold on
plot(T,K_spi,colors(i),'linewidth',1.5)
xlabel('Temperature [K]','FontSize',size)
ylabel('K [GPa]','FontSize',size)
end
leg = legend('0.0001 GPa','5 GPa','10 GPa','20 GPa','30 GPa');
set(leg,'Location','SouthWest','FontSize',10)
set(hp,'WindowStyle','docked')
set(gca,'fontsize',12)
set(hp,'PaperpositionMode','auto')
% saveas(1,'C:\Users\Stig-Erik\NTNU\Master\Latex\bulkT_MgO','epsc')
```

B.9 Bulk modulus as a function of pressure

The prediction of the bulk modulus as a function of pressure for MgO has been shown in the following script.

```
% Pseudo-Spinodal equation
% Predictions for bulk modulus as a function of pressure for MgO

clear all
close all
clc

% MgO
K01 =160.123;
K02 =3.93;
V0 = 11.25; % cm^3/mol
gamma0 = 1.49; % Speziale 2001
theta = 743*0.75;
N = 2*6.023*10^-23;
Tref = 298;

beta = 0.85;
A = beta*K01/K02;
B = K01*(1-beta);
C = A^beta;
D = 1/(1-beta);
kb = 1.38*10^23;
p = (0:1:200)';
Temp = [298.15,500,1000,2000,3000];
colors = char('blue','r','cyan','green','magenta');

for i = 1:length(Temp)
T = Temp(i);
psp298 = -K01/K02*0.85;
psp0 = psp298 - (gamma0/V0*3*N*kb*theta*(0.5+1./(exp(theta./Tref)-1)))
    /1000;
pspTref = psp0 + (gamma0/V0*3*N*kb*theta*(0.5+1./(exp(theta./Tref)-1)))
    /1000;
ha = (gamma0/V0*3*N*kb*theta*(0.5+1./(exp(theta./T)-1)))/1000;
psp = psp0 + ha;
kappa = ((-pspTref).^beta)/K01; % Calculated at Tref, independent of T
K_spi  = (1./kappa).*(p-psp).^beta; % Bulk modulus
K_spi2 = (beta./kappa).*(p-psp).^(beta-1); % Pressure derivative of
                                           % bulk modulus
Vsp = V0.*exp(beta./((1-beta)*K02));

```

```
V01 = Vsp*exp(-kappa/(1-beta).*(p-psp).^(1-beta));
V0T = Vsp*exp(-kappa/(1-beta).*(-psp).^(1-beta));
V0ref = Vsp*exp(-kappa/(1-beta).*(-pspTref).^(1-beta));

V = Vsp.*exp(-kappa/(1-beta)*(p-psp).^(1-beta));

VdivV0T = V/V0T;

a = (gamma0./(V0.*K_spi)*3*N*kb.*((theta./T).^2)).*exp(theta./T)./((exp(
    theta./T)-1).^2)/1000; % K^-1
%-------------------------------------------------------------------------
% Experimental data for alpha
h1 = load('anderson_and_zou_1989.txt');
Texp = h1(:,2);
alpha= h1(:,3)*10^-6;

%-------------------------------------------------------------------------
% Murnaghan
Kmur = K01+K02*p;
aMur = (gamma0./(V0.*Kmur)*3*N*kb.*((theta./T).^2)).*exp(theta./T)./((exp(
    theta./T)-1).^2)/1000;

% Calculating the isentropic bulk moduls
Ks = K_spi.*(1+a.*gamma0.*T);

% Plotting
size = 12;
hp = figure(1);
hold on
plot(p,K_spi,colors(i),'linewidth',1.5);
% title('Isothermal bulk modulus as a function of temperature for MgO')
xlabel('Pressure [GPa]','FontSize',size)
ylabel('K [GPa]','fontsize',12)
end
leg = legend('298.15 K','500 K','1000 K','2000 K','3000 K');
set(leg,'Location','SouthEast','FontSize',10)
set(hp,'WindowStyle','docked')
set(gca,'fontsize',12)
set(hp,'PaperpositionMode','auto')
% saveas(1,'C:\Users\Stig-Erik\NTNU\Master\Latex\bulkP_MgO','epsc')
```

B.10 Thermal expansion as a function of temperature

The prediction of the thermal expansion as a function of temperature for MgO has been shown in the following script.

```
% Pseudo-Spinodal equation
% Prediction of alpha as a unction of temperature for MgO

clear all
close all
clc

% MgO
K01 =160.123;
K02 =3.93;
V0 = 11.25; % cm^3/mol
gamma0 = 1.49; % Speziale 2001
theta = 743*0.75;
N = 2*6.023*10^-23;
Tref = 298;

beta = 0.85;
A = beta*K01/K02;
B = K01*(1-beta);
C = A^beta;
D = 1/(1-beta);
kb = 1.38*10^23;

T = (0:1:3000)';
pres = [0,5,10,20,30];
colors = char('blue','r','cyan','green','magenta');
for i = 1:length(pres)
p = pres(i);
psp298 = -K01/K02*0.85;
psp0 = psp298 - (gamma0/V0*3*N*kb*theta*(0.5+1./(exp(theta./Tref)-1)))
    /1000;
pspTref = psp0 + (gamma0/V0*3*N*kb*theta*(0.5+1./(exp(theta./Tref)-1)))
    /1000;
ha = (gamma0/V0*3*N*kb*theta*(0.5+1./(exp(theta./T)-1)))/1000;
psp = psp0 + ha;
kappa = ((-pspTref).^beta)/K01; % Calculated at Tref, independent of T
K_spi  = (1./kappa).*(p-psp).^beta; % Bulk modulus
K_spi2 = (beta./kappa).*(p-psp).^(beta-1); % Pressure derivative of
                                           % bulk modulus
Vsp = V0.*exp(beta./((1-beta)*K02));

```

```
V01 = Vsp*exp(-kappa/(1-beta).*(p-psp).^(1-beta));
V0T = Vsp*exp(-kappa/(1-beta).*(-psp).^(1-beta));
V0ref = Vsp*exp(-kappa/(1-beta).*(-pspTref).^(1-beta));

V = Vsp.*exp(-kappa/(1-beta)*(p-psp).^(1-beta));

VdivV0T = V/V0T;

a = (gamma0./(V0.*K_spi)*3*N*kb.*((theta./T).^2)).*exp(theta./T)./((exp(
    theta./T)-1).^2)/1000; % K^-1

%-------------------------------------------------------------------------
% Calculating the isentropic bulk moduls
Ks = K_spi.*(1+a.*gamma0.*T);

% Plotting
hold on
size = 12;
hp = figure(1);
% title('Thermal expansion coeffisient versus temperature for MgO')
xlabel('Temperature [K]','FontSize',size)
ylabel('\alpha [K^{-1}]','FontSize',size)
plot(T,a,colors(i),'linewidth',1.5)
hold off
end
leg = legend('0.0001 GPa','5 GPa','10 GPa','20 GPa','30 GPa');
set(leg,'Location','NorthWest','FontSize',10)
set(gca,'fontsize',12)
set(hp,'WindowStyle','docked')
set(hp,'PaperpositionMode','auto')
% saveas(1,'C:\Users\Stig-Erik\NTNU\Master\Latex\alphaT_MgO','epsc')
```

B.11 Thermal expansion as a function of pressure

The prediction of the thermal expansion as a function of pressure for MgO has been shown in the following script.

```
% Pseudo-Spinodal equation
% Prediction of alpha as a function of pressure for MgO

clear all
close all
clc

```

```
% MgO
K01 =160.123;
K02 =3.93;
V0 = 11.25; % cm^3/mol
gamma0 = 1.49; % Speziale 2001
theta = 743*0.75;
N = 2*6.023*10^-23;
Tref = 298;

beta = 0.85;
A = beta*K01/K02;
B = K01*(1-beta);
C = A^beta;
D = 1/(1-beta);
kb = 1.38*10^23;

p = (0:1:200);
Temp = [298.15,500,1000,2000,3000];
colors = char('blue','r','cyan','green','magenta');
for i = 1:length(Temp)
T = Temp(i);
psp298 = -K01/K02*0.85;
psp0 = psp298 - (gamma0/V0*3*N*kb*theta*(0.5+1./(exp(theta./Tref)-1)))
    /1000;
pspTref = psp0 + (gamma0/V0*3*N*kb*theta*(0.5+1./(exp(theta./Tref)-1)))
    /1000;
ha = (gamma0/V0*3*N*kb*theta*(0.5+1./(exp(theta./T)-1)))/1000;
psp = psp0 + ha;
kappa = ((-pspTref).^beta)/K01; % Calculated at Tref, independent of T
K_spi  = (1./kappa).*(p-psp).^beta; % Bulk modulus
K_spi2 = (beta./kappa).*(p-psp).^(beta-1); % Pressure derivative of
                                           % bulk modulus
Vsp = V0.*exp(beta./((1-beta)*K02));

V01 = Vsp*exp(-kappa/(1-beta).*(p-psp).^(1-beta));
V0T = Vsp*exp(-kappa/(1-beta).*(-psp).^(1-beta));
V0ref = Vsp*exp(-kappa/(1-beta).*(-pspTref).^(1-beta));

V = Vsp.*exp(-kappa/(1-beta)*(p-psp).^(1-beta));

VdivV0T = V/V0T;

a = (gamma0./(V0.*K_spi)*3*N*kb.*((theta./T).^2)).*exp(theta./T)./((exp(
    theta./T)-1).^2)/1000; % K^-1

%-------------------------------------------------------------------------
```

```
% Calculating the isentropic bulk moduls
Ks = K_spi.*(1+a.*gamma0.*T);

% Plotting
hold on
hp = figure(1);
% title('Thermal expansion coeffisient versus pressure for MgO')
xlabel('Pressure [GPa]','FontSize',12);
ylabel('\alpha [K^{-1}]','FontSize',12);
plot(p,a,colors(i),'linewidth',1.5)
end
leg = legend('298.15 K','500 K','1000 K','2000 K','3000 K');
set(leg,'Location','NorthEast','FontSize',10)
set(gca,'fontsize',12)
set(hp,'WindowStyle','docked')
set(hp,'PaperpositionMode','auto')
% saveas(1,'C:\Users\Stig-Erik\NTNU\Master\Latex\alphaP_MgO','epsc')
```

B.12 Comparison of the thermal expansion with experimental data

Comparsion of the thermal expansion as a function of temperature with experimental data for MgO has been shown in the following script.

```
% Pseudo-Spinodal EoS, predictions of alpha

clear all
close all
clc

% MgO
K01 =160.123;
K02 =3.93;
V0 = 11.25; % cm^3/mol
gamma0 = 1.49; % Speziale 2001
theta = 743*0.75;
N = 2*6.023*10^-23;
Tref = 298;

beta = 0.85;
A = beta*K01/K02;
B = K01*(1-beta);
C = A^beta;
```

```
D = 1/(1-beta);
kb = 1.38*10^23;
T = (0:1:3000)';
p = 0;
% T = 2000;
% p = (0:0.5:200)';

psp298 = -K01/K02*0.85;
psp0 = psp298 - (gamma0/V0*3*N*kb*theta*(0.5+1./(exp(theta./Tref)-1)))
    /1000;
pspTref = psp0 + (gamma0/V0*3*N*kb*theta*(0.5+1./(exp(theta./Tref)-1)))
    /1000;
ha = (gamma0/V0*3*N*kb*theta*(0.5+1./(exp(theta./T)-1)))/1000;
psp = psp0 + ha;
kappa = ((-pspTref).^beta)/K01; % Calculated at Tref, independent of T
K_spi  = (1./kappa).*(p-psp).^beta; % Bulk modulus
K_spi2 = (beta./kappa).*(p-psp).^(beta-1); % Pressure derivative of
                                           % bulk modulus
Vsp = V0.*exp(beta./((1-beta)*K02));

V01 = Vsp*exp(-kappa/(1-beta).*(p-psp).^(1-beta));
V0T = Vsp*exp(-kappa/(1-beta).*(-psp).^(1-beta));
V0ref = Vsp*exp(-kappa/(1-beta).*(-pspTref).^(1-beta));

V = Vsp.*exp(-kappa/(1-beta)*(p-psp).^(1-beta));

VdivV0T = V/V0T;

a = (gamma0./(V0.*K_spi)*3*N*kb.*((theta./T).^2)).*exp(theta./T)./((exp(
    theta./T)-1).^2)/1000; % K^-1
%-------------------------------------------------------------------------
% Experimental data for alpha
h1 = load('anderson_and_zou_1989.txt');
Texp = h1(:,2);
alpha= h1(:,3)*10^-6;

%-------------------------------------------------------------------------
% Murnaghan
Kmur = K01+K02*p;
aMur = (gamma0./(V0.*Kmur)*3*N*kb.*((theta./T).^2)).*exp(theta./T)./((exp(
    theta./T)-1).^2)/1000;

% Calculating the isentropic bulk moduls
Ks = K_spi.*(1+a.*gamma0.*T);

% Plotting
```

```
hold on
hp = figure(1);
axis([0 3000 0 0.00008])
xlabel('Temperature [K]')
ylabel('\alpha(T)_{p_0}')
plot(T,a,'linewidth',1.5)
plot(T,aMur, 'r','linewidth',1.5)
plot(Texp,alpha,'*')
hold off
set(hp,'WindowStyle','docked')
set(hp,'PaperpositionMode','auto')
leg = legend('Pseudo-spinodal','First order Murnaghan', 'Exp. data');
set(leg,'Location', 'SouthEast')
saveas(1,'C:\Users\Stig-Erik\NTNU\Master\Latex\alphaTexp_MgO.pdf')
```

B.13 Comparison of the p-V-T surface with experimental data for MgO

Comparsion of the pressure-volume-temperature surface with experimental data for MgO has been shown in the following script.

```
% Comparison of the p-s EoS versus experimental data

clear all
close all
clc

K01 =160.123;
K02 =3.93;
V0 = 11.25; % cm^3/mol
gamma0 = 1.49; % Speziale 2001
theta = 743*0.75;
N = 2*6.023*10^-23;
kb = 1.38*10^23;
Tref = 298;

beta = 0.85;

% T = (0:5:1200)';
% p = 0;
Temp = [298,1100];
p = (0:0.5:220)';
colors = char('blue','r','cyan','green','yellow','magenta');
```

```
for i = 1:length(Temp)
    T = Temp(i);
psp298 = -K01/K02*0.85;
psp0 = psp298 - (gamma0/V0*3*N*kb*theta*(0.5+1./(exp(theta./Tref)-1)))
    /1000;
pspTref = psp0 + (gamma0/V0*3*N*kb*theta*(0.5+1./(exp(theta./Tref)-1)))
    /1000;
ha = (gamma0/V0*3*N*kb*theta*(0.5+1./(exp(theta./T)-1)))/1000;
psp = psp0 + ha;
kappa = ((-pspTref).^beta)/K01; % Calculated at Tref, independent of T
K_spi  = (1./kappa).*(p-psp).^beta; % Bulk modulus
K_spi2 = (beta./kappa).*(p-psp).^(beta-1); % Pressure derivative of
                                           % bulk modulus
Vsp = V0.*exp(beta./((1-beta)*K02));

V01 = Vsp*exp(-kappa/(1-beta).*(p-psp).^(1-beta));
V0T = Vsp*exp(-kappa/(1-beta).*(-psp).^(1-beta));
V0ref = Vsp*exp(-kappa/(1-beta).*(-pspTref).^(1-beta));

V = Vsp.*exp(-kappa/(1-beta)*(p-psp).^(1-beta));

VdivV0 = V/V0ref;

a = (gamma0./(V0.*K_spi)*3*N*kb.*((theta./T).^2)).*exp(theta./T)./((exp(
    theta./T)-1).^2)/1000; % K^-1

% Murnaghan
KMur = K01+K02*p;
aMur = (gamma0./(V0.*KMur)*3*N*kb.*((theta./T).^2)).*exp(theta./T)./((exp(
    theta./T)-1).^2)/1000;
aKT =-aMur.*KMur; % GPaK^(-1)
Pth = aKT.*(T-Tref);
p0 = 0.0001;
pmur = p+Pth;
VdivV0Mur = ((K01+K02*pmur)./(K01+K02*p0)).^(-1/K02);
%-------------------------------------------------------------------------
% Experimental data for alpha
h1 = load('Speziale_and_Zha_etal_2001.txt');
pexp = h1(:,3);
VdivV0exp= h1(:,4);
h2 = load('fei_1999.txt');
pexp2 = h2(:,3);
VdivV0exp2 = h2(:,4)/h2(1,4);

%-------------------------------------------------------------------------
% Plotting
```

```
axis([0 25 0.85 1.1])
hp = figure(1);
hold on
xlab = xlabel('p [GPa]');
ylabel('V/V_0')
    plot(p,VdivV0,colors(i), 'linewidth', 1.5)
end
plot(pexp2,VdivV0exp2,'*')
legend('298 K','1100 K','Exp. data');
% set(gca,'FontSize',10)
set(hp,'WindowStyle','docked')
set(hp,'PaperpositionMode','auto')
saveas(1,'C:\Users\Stig-Erik\NTNU\Master\Latex\pvt_MgO','epsc')
```

B.14 Calculation of the Chi-square value for MgO

Comparsion of the pressure-volume-temperature surface with experimental data for MgO has been shown in the following script.

```
% Test of MgO data

clear all
close all
clc

addpath(cd('..\'));
K01 =160.123;
K02 =3.93044;
K03 =-0.00269764;
[p, VdivV0] = pvdata_mgo();
x4 = [K01 K02 K03];
xdata4 = [VdivV0', p']';
param = struct('len', 0);
F4 = newcurve_res_mgo(x4,xdata4,param);
F4 = F4(1:length(F4)/2);
% Standarizing the data
stdav = sqrt(var(F4));
my = mean(F4);
Fsort4 = sort((F4-my)/stdav);
y4 = (1:length(F4))/length(F4);
hold on
% title('Cumulative plot MgO')
plot(Fsort4,y4, '+')
clear path
```

```
% Plot the cumulative normal distribution
normdist = -3:0.1:3;
p1 = cdf('Normal',normdist,0,1);
axis([-3 3 0 1])
ylabel('\Phi(x)','fontsize',14)
xlabel('x','fontsize',14)
plot(normdist,p1)
bins2 = -2:0.5:2;
bins = [bins2,6];
cumE = 0;
cumO = 0;
O = zeros(10,1);
E = zeros(10,1);
for i = 1:10
O(i) = length(find(Fsort4<bins(i)))-cumO;
cumO = cumO+O(i);
E(i) = (p1(max(find(normdist<=bins(i))))-cumE);
cumE = cumE+E(i);
end
E = E*(length(Fsort4)-5);
Exp = zeros(length(E),1);
Obs = zeros(length(O),1);
for i = 1:length(E)/2
    if E(i)<5
        Exp(i+1)=Exp(i)+E(i);
        Obs(i+1)=Obs(i)+O(i);
        Exp(i)=0;
        Obs(i)=0;
    else
        Exp(i)=Exp(i)+E(i);
        Obs(i)=Obs(i)+O(i);
    end
end

for i = length(E)/2+1:length(E)
    if E(i)<5
        Exp(i)=0;
        Obs(i)=0;
     else
        Exp(i)=Exp(i)+E(i);
        Obs(i)=Obs(i)+O(i);
     end
end
Exp(9)=E(10)+E(9);
Obs(9)=O(10)+O(9);
for i = 1:length(Exp)
```

```
72      if Exp(i)>0
73          chi(i) = (Obs(i)-Exp(i))^2/(Exp(i));
74      end
75  end
76  sumchi = sum(chi);
77  disp(sumchi)
```